Accepted to the Astrophysical Journal: August 12, 2004
Preprint typeset using LaTeX style emulateapj v. 20/04/00

PROBING THE IGM/GALAXY CONNECTION TOWARD PKS0405-123 I: UV SPECTROSCOPY AND METAL-LINE SYSTEMS

Jason X. Prochaska[1], Hsiao-Wen Chen[2,3], J. Christopher Howk[4], Benjamin J. Weiner[1], and John Mulchaey[5]

Accepted to the Astrophysical Journal: August 12, 2004

ABSTRACT

We present results from an analysis of *Far Ultraviolet Spectroscopic Explorer* (FUSE) spectroscopy of the $z_{em} = 0.57$ quasar PKS0405–123. We focus on the intervening metal-line systems identified along the sightline and investigate their ionization mechanism, ionization state, and chemical abundances. Including HST/STIS spectroscopy, we survey the entire sightline and identify six O VI absorbers to a 3σ equivalent width (EW) limit of 60mÅ. This implies an incidence $dN/dz = 16^{+9}_{-6}$ consistent with previous O VI studies. In half of the O VI systems we report positive detections of C III suggesting the gas is predominantly photoionized, has multiple ionization phases, or is in a non-equilibrium state. This contrasts with the general description of the warm-hot intergalactic medium (WHIM) as described by numerical simulations where the gas is predominantly in collisional ionization equilibrium. An appreciable fraction of O VI absorbers may therefore have a different origin. We have also searched the sightline for the Ne VIII doublet over the redshift range $0.2 < z < z_{em}$ which is a better probe of the WHIM gas at $T > 10^6$ K. We find no positive detections to an EW limit of 80mÅ giving $dN/dz < 40$ at 95% c.l.

The photoionized metal-line systems exhibit a correlation between the ionization parameter ($U = \Phi/cn_H$ with Φ the flux of hydrogen ionizing photons) and H I column density for $N(\mathrm{HI}) = 10^{14} - 10^{16}\,\mathrm{cm}^{-2}$. Both the slope and normalization of this correlation match the prediction inferred from the results of Davé and Tripp for the low z Lyα forest. In turn, the data show a tentative, unexpected result: five out of the six photoionized metal-line systems show a total hydrogen column density within a factor of 2 of $10^{18.7}\,\mathrm{cm}^{-2}$. Finally, the median metallicity [M/H] of twelve $z \sim 0.3$ absorbers with $N(\mathrm{HI}) > 10^{14}\,\mathrm{cm}^{-2}$ is [M/H] > -1.5 with large scatter. This significantly exceeds the median metallicity of C IV and O VI systems at $z \sim 3$. and therefore requires enrichment of the intergalactic medium over the past ≈ 10 Gyr.

Subject headings: Intergalactic medium

1. INTRODUCTION

Quasar absorption line studies examine the gas within galaxies and the intergalactic medium (IGM) between them. These studies include analyze of the interstellar medium of young galaxies at $z > 2$ (e.g. the damped Lyα systems) as well as the lines that comprise the Lyα forest. One of the most notable successes of cold dark matter cosmologies at $z \sim 3$ is the general agreement between observations of the Lyα forest and cosmological simulations both in terms of the column density and Doppler width distributions (e.g. Miralda-Escudé et al. 1996; Zhang et al. 1997). Meanwhile, analyses of metal-line systems describe the enrichment history of the universe (Pettini et al. 1997; Prochaska et al. 2003), test processes of nucleosynthesis (e.g. Lu et al. 1996; Prochaska, Howk, & Wolfe 2003), and examine the role and characteristics of winds (Aguirre et al. 2001) and Population III enrichment (Gnedin & Ostriker 1997; Wasserburg & Qian 2000).

The 'fluctuating Gunn-Peterson' paradigm inferred from numerical simulations describes the majority of the observed IGM as large-scale overdensities with little correspondence to individual galaxies (e.g Gnedin & Hui 1998). Although this model reasonably reproduces the number density and gross kinematics of the IGM, it has not been extensively tested by observations. This is especially true at low redshift where there are very few sightlines with high resolution, high quality spectra. For this reason, alternative models (e.g. absorption by gas in galactic halos or low surface brightness galaxies; Linder 2000; Chen, Lanzetta, & Webb 2001; Manning 2003) are generally as successful at explaining the low z IGM as the CDM paradigm (Davé & Tripp 2001).

We are pursuing an observing program aimed at addressing key questions related to the low z IGM. We have chosen to study the IGM along the sightlines to $z > 0.1$ AGN with relatively high signal-to-noise (S/N) far-UV FUSE spectroscopy and, in many cases, HST/STIS echelle observations. This UV spectroscopy is complemented by large field of view ($> 20'$ diameter) galaxy surveys compiled with the WFCCD spectrograph at Las Campanas Observatory. The principal focus of our program is to identify the location and physical characteristics of low redshift O VI absorbers, whose hot gas content is believed to be a significant reservoir of baryons (Cen & Ostriker 1999; Tripp et al. 2000; Davé et al. 2001; Fang & Bryan 2001). The properties in which we are interested include the ionization state, metallicity, and absorber/galaxy cross-correlation function for O VI gas. Studies of the O VI absorbers currently provide the most efficient means of studying the relatively hot $T \approx 10^{5-7}$K, low density gas termed the

[1]UCO/Lick Observatory; University of California, Santa Cruz; Santa Cruz, CA 95064; xavier@ucolick.org

[2]Center for Space Research, Massachusetts Institute of Technology, Cambridge, MA 02139-4307; hchen@mit.edu

[3]Hubble Fellow

[4]Department of Physics, and Center for Astrophysics and Space Sciences, University of California, San Diego, C–0424, La Jolla, CA 92093-0424

[5]Observatories of the Carnegie Institution of Washington, 213 Santa Barbara St., Pasadena, CA 91101

warm-hot intergalactic medium (WHIM). The WHIM is predicted to contain a large fraction of the baryons at low z (Davé et al. 2001), but its existence is difficult to verify due to its low density. In addition to studies on the origin of the WHIM, the combined datasets of high quality UV spectroscopy and deep, large field-of-view galaxy surveys will examine several aspects of the IGM/galaxy connection. These issues are intimately related to our understanding of gas and galaxies in the local universe. Through comparisons with hydrodynamic numerical simulations, we will test and constrain the CDM paradigm for the IGM and examine processes of galaxy feedback and chemical enrichment.

This paper focuses on the metal-line absorbers identified in the ultraviolet spectroscopy of PKS0405–123. We have focused first on the PKS0405–123 sightline for the following reasons: (i) It exhibits one of the brightest UV fluxes for a $z > 0.5$ quasar. This allowed the STIS science team to obtain high quality UV spectroscopy from $\lambda \approx 1200 - 1700$Å and our team to acquire modest S/N FUV spectroscopy from $\lambda \approx 900 - 1170$Å with the FUSE Observatory. (ii) It exhibits a partial Lyman limit system (i.e. an absorber with $\tau \lesssim 1$ at $\lambda_{rest} = 912$Å) at $z = 0.167$ (Chen & Prochaska 2000). In this paper we report on our analysis of the UV spectroscopy and examine the metal-line systems identified along this sightline. and (iii) We have composed a $\approx 1\square^\circ$ galaxy survey reaching $R \lesssim 20$ with ≈ 500 galaxies at $z < z_{em}$. Concurrent and forthcoming papers on this sightline will (a) report on the physical nature of the absorber identified at $z = 0.4951$ (Howk et al. 2004), (b) describe the galaxy survey and the connection between galaxies and the metal-line systems discussed here (Prochaska et al. 2004); and (c) present an analysis of the Lyα/galaxy cross-correlation function (Chen et al. 2004). Future work will analyze the IGM and the galaxies associated with it for ≈ 10 low redshift fields.

The paper is organized as follows: in § 2 we present the FUSE observations and a line list of significant absorbers identified along the sightline; in § 3 we describe our approach to ionization modeling; we analyze the ionization state, physical conditions and elemental abundances of the metal-line systems in § 4; § 5 lists the absorbers along the sightline with $N(\mathrm{HI}) > 10^{14}\,\mathrm{cm}^{-2}$ which do not display metal transitions; we discuss the implications of our results for the WHIM, chemical enrichment, and the general IGM in § 6; and § 7 gives a brief summary.

Table 1
UV SPECTROSCOPY

Instr.	Mode	Wavelength	Exp.	S/N[a]
FUSE	LWRS	900–1180Å	71ks	5-15
HST/STIS	E140M	1150–1700Å	27ks	7

[a]Signal-to-noise per resolution element for *FUSE* data and per pixel for HST/STIS.

2. OBSERVATIONS, DATA REDUCTION, AND EW ANALYSIS

PKS0405–123 was observed for 71ks during Cycle 2 of the FUSE mission (Program B087; PI: Prochaska). This program was principally motivated by the identification of a strong metal-line system at $z = 0.167$ in the HST+STIS/E140M data of PKS0405–123 obtained by the STIS science team (Williger et al. 2004). In Chen & Prochaska (2000), we analyzed this absorption system and argued that it is a partial Lyman limit system with roughly solar metallicity. We then obtained far-UV spectroscopy with the FUSE observatory to further constrain the physical characteristics of this absorber. Table 1 summarizes the UV spectroscopy acquired with FUSE and HST/STIS of PKS0405–123 and estimates the signal-to-noise (S/N) per resolution element.

Table 2
ATOMIC DATA

Transition	λ	f	Ref
HI 972	972.5368	0.029	1
OI 988a	988.5778	0.0005146	1
OI 988b	988.6549	0.007712	1
OI 988	988.7734	0.04318	1
NIII 989	989.7990	0.1066	1
SiII 989	989.8731	0.133	1

References. — Key to References – 1: Morton (1991); 2: Howk et al. (20
Lawler (1999); 7: Fedchak, Wiese, & Lawler (2000); 9: Schectman, Povolny,
Fedchak, & Lawler (2001); 13: Bergeson & Lawler (1993); 14: Bergeson, Mul
Mullman, & Lawler (1996)

Note. — [The complete version of this table is in the electronic edition of th

Table 3
ADOPTED SOLAR ABUNDANCES

Elm	$\epsilon(X)^a$	Z
H	12.00	1
C	8.59	6
N	7.93	7
O	8.74	8
Ne	8.08	10
Mg	7.58	12
Al	6.49	13
Si	7.56	14
S	7.20	16
Fe	7.50	26

[a]$\epsilon(X)$ is the logarithmic number density of a given element scaled such that $\epsilon(\mathrm{H}$

PKS0405–123 was observed with the FUSE observatory (Moos et al. 2000; Sahnow et al. 2000) using the LWRS apertures with the detectors in TTAG mode during one visit beginning UT 05 October 2001. We used *ttag_combine* to concatenate the photon event lists into a single file and then processed this file with the CalFUSE pipeline (v2.4). The reduction proceeded without any significant warnings and the standard series of output files was created. We binned these data arrays by three 'pixels' (≈ 0.028Å per bin) and then traced the continuum of PKS0405–123 in each channel separately by fitting Legendre polynomials to regions of unabsorbed quasar continuum. These normalized spectra form the dataset for

TABLE 4
EW SUMMARY

Ion	λ_{obs} (Å)	λ_{rest} (Å)	z_{abs}	W_1 (mÅ)	$\sigma(W_1)$ (mÅ)	W_2 (mÅ)	$\sigma(W_2)$ (mÅ)	W_f (mÅ)	$\sigma(W_f)$ (mÅ)
FUSE									
OIV 787	931.521	787.711	0.18257	7	15	42	12	28	9
OIV 787	931.797	787.711	0.18292	124	17	131	14	128	11
MgX 624	934.389	624.950	0.49514	−2	13	−12	10	−8	8
OV 629	941.457	629.730	0.49502	183	12	145	12	164	9
SIV 809	944.893	809.668	0.16701	13	16	31	15	23	11
OII 834	973.896	834.466	0.16709	8	17	17	12	14	10
OIII 832	985.062	832.927	0.18265	34	15	5	11	15	9

Note. — Note that the list is incomplete for wavelengths < 1000Å where the data has poor S/N and significant line blending.

Note. — Columns 4,5 (6,7) refer to the SiC1B (SiC2A) channel for 910Å< λ < 990Å, LiF1A (LiF2B) for 995Å< λ < 1057Å, LiF1A for 1057Å< λ < 1082Å, LiF2A for 1082Å< λ < 1100Å, LiF1B (LiF2A) for 1100Å< λ < 1180Å, and STIS/E140M for λ > 1190Å.

Note. — [The complete version of this table is in the electronic edition of the Journal. The printed edition contains only a sample.]

our analysis. The atomic data considered in this paper is tabulated in Table 2 and Table 3 lists our assumed solar abundance data compiled by Grevesse & Sauval (1999) and revised by Holweger (2001) for C,N, and O.

Redward of 1000Å, we identified all 3σ features in the LiF1A and LiF2A channels. There is moderate absorption from Galactic molecular hydrogen along this sightline; we attribute $\approx$ 50% of the features at $\lambda = 1000 - 1150$Å to H_2 or Galactic metal-line transitions. Table 4 lists the observed wavelength, transition name, absorption redshift, rest equivalent width W_λ, and the statistical error in W_λ from each channel where the transition is observed at reasonable S/N. Columns 4,5 (6,7) refer to the SiC1B (SiC2A) channel for 910Å< λ < 990Å, LiF1A (LiF2B) for 995Å< λ < 1057Å, LiF1A for 1057Å< λ < 1082Å, LiF2A for 1082Å< λ < 1100Å, LiF1B (LiF2A) for 1100Å< λ < 1180Å, and STIS/E140M for λ > 1190Å (see Chen & Prochaska 2000 for details of the STIS dataset and reduction). Note that there are offsets between the wavelength solutions for each FUSE channel. We corrected for these offsets with a cross-correlation analysis allowing for a zero point and a first order term. The latter term, while small, is required to match the spectrum over the entire spectral range of each channel. This procedure only corrects for relative errors; a comparison of H I Lyman lines and metal lines from the STIS and FUSE spectra indicates the absolute wavelength calibration is accurate to better than 10 km s^{-1} . The final columns in Table 4 list the adopted W_λ value and uncertainty corresponding to the variance weighted mean for transitions with multiple measurements. In general, the values derived from multiple channels show good agreement. For several transitions (e.g. Galactic P II 1152), however, the individual W_λ values differ by > 3σ statistical significance. In most cases, this may be attributed to fixed pattern noise in the detectors or continuum uncertainties. The transitions showing these discrepant cases were either ignored or we adopted an uncertainty equal to the spread in the two values.

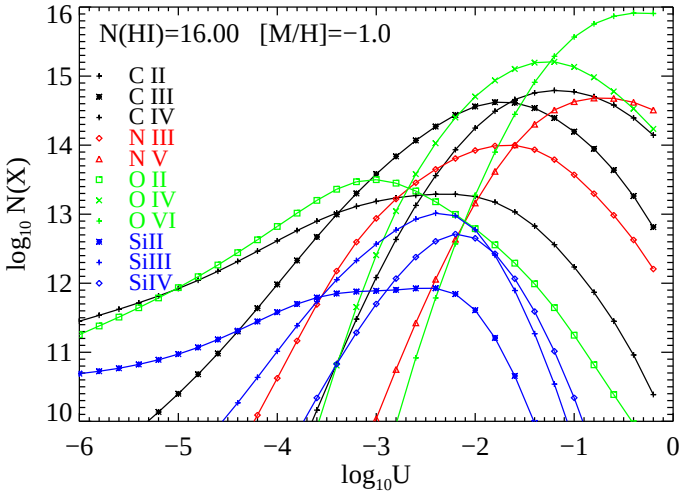

FIG. 1.— Predicted ionic column densities for a photoionized gas as a function of ionization parameter U. The curves are the results of a series of calculations with the Cloudy software package (Ferland 2001) assuming (i) a quasar-only extragalactic UV background (model Q) at $z = 0$; (ii) a total H I column density $N(\mathrm{HI}) = 10^{16}$ cm^{-2}; and (iii) solar relative abundances scaled to a metallicity of 1/10 solar.

3. IONIZATION MODELING

3.1. *Photoionization*

In this paper, we examine gas likely to be significantly ionized. For those systems which show multiple ionic species, it is possible to constrain the ionization mechanism (i.e. photoionization vs. collisional ionization) and ionization state of the gas. In general, we expect the gas to be significantly photoionized, either by an extragalactic UV background (EUVB) radiation field or a local radiation source (e.g. proximity to a starbursting galaxy). For the shape of the EUVB field, we consider two models generated by Haardt & Madau (2004) using their CUBA software package: quasar-only (Q) and quasars+galaxies

(QG). These models input the luminosity function of AGN and UV bright galaxies for a given redshift and then calculate the attenuation of the mean intensity by the intergalactic medium. The majority of previous studies have adopted model Q for the EUVB field. In our analysis, we will consider this model as the default spectrum, and we note that ongoing programs studying the UV emission of low z galaxies (e.g. GALEX) will provide a more accurate assessment of the proper EUVB model. Where relevant, we describe the effects of including a softer radiation field than model Q.

In practice we calculate solutions for a plane-parallel slab of gas using the Cloudy software package (Ferland 2001). Because all of the absorbers along the PKS0405–123 sightline are optically thin to the radiation field, the calculation is simplified and the models are fully described by (i) the ionization parameter $U \equiv \Phi/cn_H$, with Φ the flux of hydrogen ionizing photons and n_H the volume density of hydrogen; (ii) the shape of the ionizing radiation field; and (iii) the metallicity of the gas [M/H]. The models are most sensitive to variations in the ionization parameter while the shape of the radiation field and the gas metallicity play more modest roles. Throughout the analysis we assume constant density (typically an arbitrary $\log n_H = -1$) and constrain the plane-parallel slab to have the thickness required to yield the observed N(HI) value given the specific ionization state of the gas.

We have constructed grids of these photoionization models varying U, [M/H], and the EUVB model for a range of redshifts and N(HI) values. An example of one set of models is shown in Figure 1 where we have assumed EUVB model Q at $z = 0$ and $N(\mathrm{HI}) = 10^{16}\,\mathrm{cm}^{-2}$. The lines trace predicted ionic column densities vs. $\log U$ for a series of ions in a gas with 1/10 solar metallicity (i.e. [M/H] = −1) and solar relative abundances (Table 3). Low-ion species (e.g. Si II) show less variation at $\log U < -3$ because they trace the H I gas to first order and the models assume a fixed N(HI) value. In contrast, high-ion species show large values only for higher ionization parameters.

The general effect of adopting a softer radiation field (e.g. EUVB model QG) is that one requires a higher ionization parameter to attain significant column densities of O IV,O V, etc. In turn, higher U values imply lower neutral fractions and therefore larger N(H) values for a fixed (observed) N(HI) value which – contrary to our initial expectation – predicts lower metallicities ($\approx 0.3 - 0.5$ dex lower) for absorbers dominated by high-ions. Systems characterized by a mixture of low and intermediate ions, however, show minimal differences in their elemental abundances as a function of the EUVB model.

Our general approach for a given absorber is to (1) constrain U with one or more ionic ratios, ideally of the same element (e.g. N(Si II)/N(Si III)); (2) determine if a self-consistent solution is allowed with all of the ions included; and (3) estimate the ionization parameter, metallicity, relative abundances, and physical conditions (e.g. density, temperature) of the gas from the best ionization model. This technique is dominated by systematic error, e.g. the limited constraints on the EUVB model, the simplifying assumption of constant density, etc. With current model sophistication and typical observational constraints, we do not believe one can achieve better than 0.2–0.3 dex precision on elemental abundances or 0.2 dex for relative abundances. Therefore, we take a cautious approach when comparing the observations against the photoionization models and adopt conservative errors.

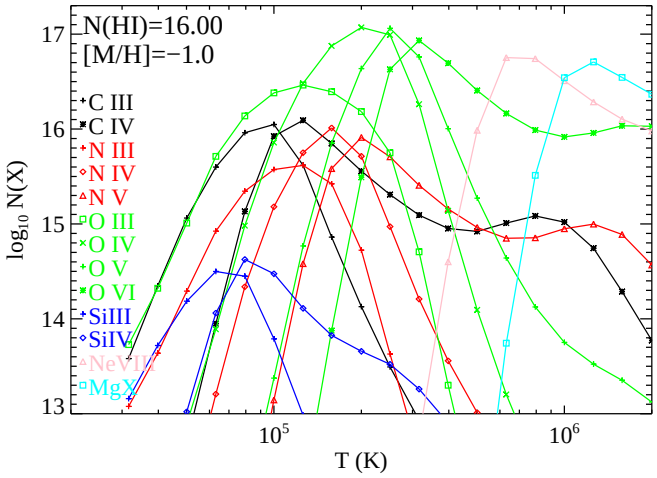

FIG. 2.— Predicted ionic column densities for a collisionally ionized gas in equilibrium as a function of gas temperature T. The curves were calculated with the Cloudy software package assuming (i) no ionizing radiation field; (ii) $N(\mathrm{HI}) = 10^{16}\,\mathrm{cm}^{-2}$; and (iii) solar relative abundances scaled to a metallicity of 1/10 solar.

3.2. *Collisional Ionization*

For gas at relatively high temperatures ($T > 5 \times 10^4$ K), collisional ionization can be the dominant ionization process for a number of high-ions observed in quasar absorption line systems (e.g. C IV, N V, O VI). In Figure 2 we plot abundance curves vs. temperature under the assumption of collisional ionization equilibrium (CIE; Sutherland & Dopita 1993) as calculated by the Cloudy package. We have assumed 1/10 solar metallicity and plot the predicted column densities for several ions assuming $N(\mathrm{HI}) = 10^{16}\,\mathrm{cm}^{-2}$ and solar relative abundances (Table 3). Collisional ionization is important for higher ionization states of Si and C at $T \approx 5 \times 10^4 - 2 \times 10^5$ K whereas O and N become highly ionized at $T \approx 10^5 - 10^6$ K. There are several key differences between the curves presented in Figures 1 and 2 which direct our discussion on the ionization mechanism of the metal-line systems toward PKS0405–123. In particular, note that the C III and O VI ions do not coexist with significant values in the collisional ionization solutions yet both ions show large column densities for $\log U \approx -1.5$ in the photoionization model. A similar difference is noted for N III. In addition, the relative abundances of the individual O ions show modest differences in the two models, e.g. photoionization tends to predict smaller differences between N(O IV) and N(O VI) than collisional ionization. Another key difference between the two scenarios is temperature of the gas: CIE models generally predict much higher temperature. Therefore, the Doppler width (b value) of the absorption can provide a discriminant between the two scenarios, especially when the neutral hydrogen gas shows $b < 30$ km s^{-1}.

3.3. *Multi-phase Scenarios and Other Ionization States*

If one is limited to the observation of only a handful of ions, however, it may be difficult to distinguish between a gas with an ionization phase dictated by photoionization versus collisional ionization. For example, a CIE model with $T \approx 2 \times 10^5$ K predicts similar relative ionic column densities of O VI and N V as a photoionization model with $\log U > -1$. In these cases, degenerate solutions exist which limit our constraints on the physical properties of the gas. Furthermore, the ionization mechanisms are not exclusive. For the absorbers considered in this paper, one expects that a radiation field is always present and a pure CIE model is somewhat unrealistic (although the effects of photoionization may be minor). In the following section, our approach will be to assess single-phase ionization models first and only consider multi-phase scenarios as required by the observations.

There are also examples in the literature of ionized gas which is not well explained by equilibrium models of collisional or photionization. The best-known examples of non-equilibrium gas involve gas in the interstellar medium of galaxies at temperatures where the cooling rate is extremely high, including T 10^5 K gas studied through lines from the Li-like ions O VI, N V, and C IV. The prevailing conclusion is that this gas is not in equilibrium and arises as a result of conductive heating, radiative shocks, and/or turbulent mixing layers (see Spitzer 1996 for a summary). Models of these phenomena predict a wide range of gas properties and diagnostics dependent on the assumed initial conditions and timescales for cooling, heating, and mixing. In this paper, we will restrict our analysis equilibrium models of collisional and photoionization. In part, this is because we have very few measurements of C IV and Si IV for these absorbers. More importantly, examples of conduction heating and radiative shocks are more likely to occur in dense, star forming regions; such conditions are unlikely for the absorption systems considered here. Finally, we will find that the systems are well described by a single or two-phase equilibrium model. Nevertheless, it is important to stress that our results are sensitive to the presumption of equilibrium modeling.

4. ANALYSIS OF THE METAL-LINE SYSTEMS

This section presents an analysis of all of the metal-line systems identified along the sightline to PKS0405–123. Because of the complicated line-spread functions of the spectrographs, we derive the N(HI) values and Doppler parameters for the H I gas using a curve-of-growth (COG) analysis. For the metal-line transitions, we report rest-frame equivalent widths, column densities calculated using the apparent optical depth method (AODM; Savage and Sembach 1991; Jenkins 1996), and statistical errors for 3σ significant transitions. At FUSE resolution, the majority of weak transitions are free of significant line saturation and the AODM approach should give accurate column densities. The technique has the added advantage that the values are free of the parametric modeling inherent to line-profile fitting. In general, upper limits reflect 2σ statistical limits and lower limits signify probable line saturation. We identify each system by a redshift which corresponds to the centroid of the hydrogen Lyman series or the peak optical depth of the metal-line transitions. Throughout this section, the data plotted are from the SiC2A, LiF1A, and LiF2A channels or the STIS instrument. For the velocity plot profiles, we indicate blends with coincident absorption lines (primarily Galactic H_2) as dotted orange lines.

We caution that this section is quite detailed. The casual reader may wish to skip to the summary table presented at the end of the section.

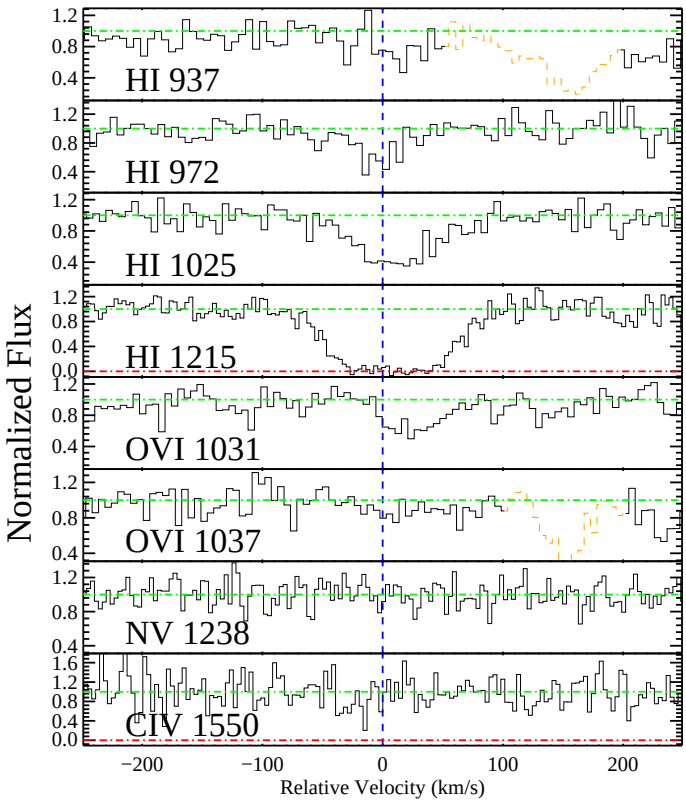

FIG. 3.— Velocity profiles of the Lyman series and metal-line transitions analyzed for the absorption system at $z = 0.09180$. In this and the following velocity profile plots, the dotted orange lines denote blends from coincident transitions and the dash-dot red line indicates the zero level.

TABLE 5
IONIC COLUMN DENSITIES FOR THE ABSORBER AT z=0.09180

Ion	λ (Å)	EW (mÅ)	AODM	N_{adopt}
HI				14.52 ± 0.05
CIV	1550.7700	< 49	< 13.70	< 13.70
NV	1238.8210	< 20	< 13.15	< 13.15
OVI	1031.9261	73 ± 8	13.82 ± 0.05	13.83 ± 0.04
OVI	1037.6167	38 ± 10	13.83 ± 0.11	

4.1. $z = 0.09180$

The lowest redshift metal-line system identified toward PKS0405–123 is an O VI system at $z = 0.0918$. Both transitions of the O VI doublet are detected and give a column density N(O VI) = $10^{13.8\pm0.04}$ cm^{-2} (Table 5). The

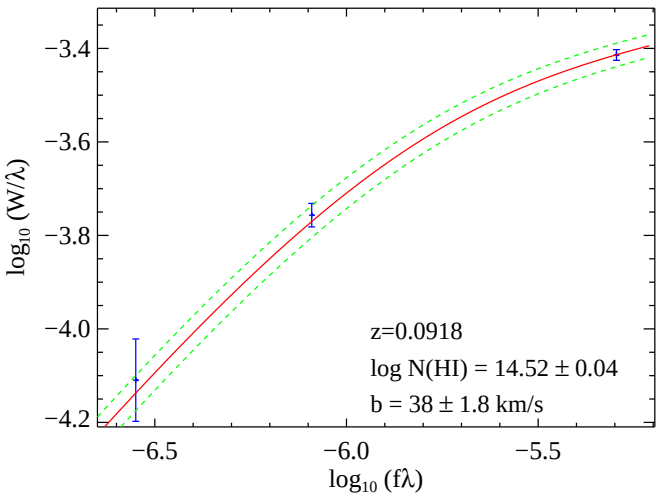

FIG. 4.— Curve-of-growth analysis of the Lyman series for the gas at $z = 0.09180$.

STIS+FUSE spectra reveal H I transitions for Lyα, Lyβ, Lyγ, and a marginal Lyϵ detection (Figure 3). The results of a COG analysis are presented in Figure 4. Minimizing χ^2 for the W$_\lambda$values as a function of $f\lambda$, we derive $N(\mathrm{HI}) = 10^{14.52\pm0.04}\,\mathrm{cm}^{-2}$ and $b = 38 \pm 2\,\mathrm{km\ s}^{-1}$.

Unfortunately, the C III 977 transition for this absorber is blended with the Lyman series of the metal-line system at $z = 0.167$. As noted above (§ 3), C III is particularly valuable for evaluating the ionization mechanism of O VI absorbers. With only a limited set of ionic column densities for this absorber, both CIE and photoionization solutions are allowed although the non-detection of N V places tight constraints on the temperature and ionization parameter. For collisional ionization equilibrium, the upper limit to $N(\mathrm{N\,V})/N(\mathrm{O\,VI})$ sets a lower limit to the temperature of $T > 2.5 \times 10^5$K assuming [N/O] > -0.5 dex. This temperature is roughly consistent with the Doppler parameter measured for the H I gas ($b \approx 40\,\mathrm{km\ s}^{-1}$). We also note that the O VI profile is offset by $\approx +20\,\mathrm{km\ s}^{-1}$ from the centroid of the H I profile. Perhaps the O VI gas is related to a more tenuous H I component. At the least, the kinematics raise the likelihood that this is a multi-phase absorber.

For photoionization (EUVB model Q), the $N(\mathrm{N\,V})/N(\mathrm{O\,VI})$ limit restricts the ionization parameter $\log U >$ [N/O] $- 1.1$. Assuming [N/O] $= 0$ and $J_{912} = 2 \times 10^{-23}$ this implies a gas density $n_H < 3 \times 10^{10^{-5}}\,\mathrm{cm}^{-3}$ which is consistent with the volume density for absorbers with $N(\mathrm{HI}) \approx 10^{14.5}\,\mathrm{cm}^{-2}$ predicted by numerical simulations (e.g. Davé et al. 2001). In addition, this implies an absorber size $\ell > 30\,\mathrm{kpc}$.

We can place a lower limit to the O/H metallicity by considering the minimum O VI/H I ionization correction. This gives [O/H] > -1.4 for photoionization and [O/H] > -2.2 for collisional ionization. Note that these are strict lower limits because we have assumed all of the observed H I gas is associated with the O VI absorber.

4.2. $z = 0.09658$

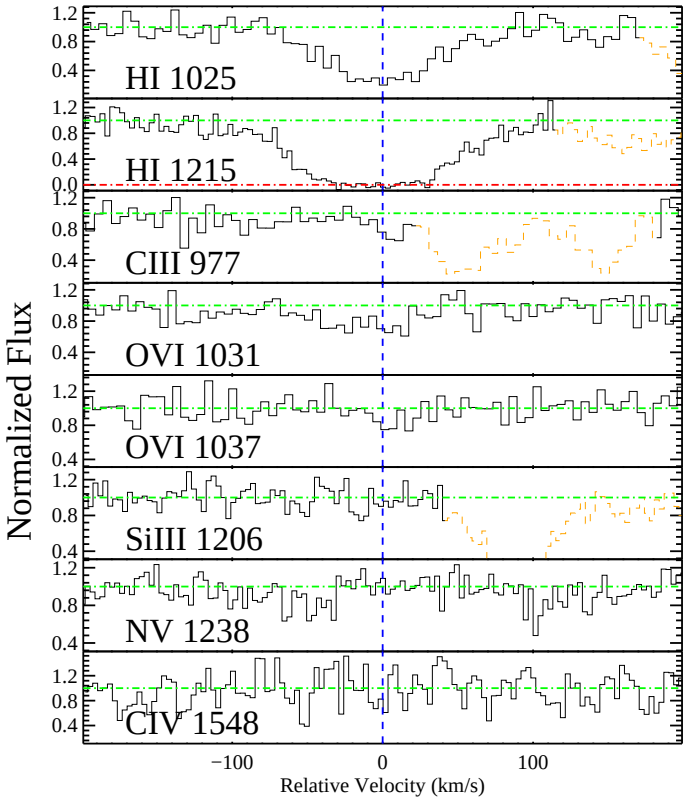

FIG. 5.— Velocity profiles of the Lyman series and metal-line transitions analyzed for the absorption system at $z = 0.09658$.

TABLE 6
IONIC COLUMN DENSITIES FOR THE ABSORBER AT z=0.09658

Ion	λ (Å)	EW (mÅ)	AODM	N_{adopt}
HI				14.65 ± 0.05
CIII	977.0200	26 ± 7	12.68 ± 0.12	12.68 ± 0.12
CIV	1548.1950	< 53	< 13.30	< 13.30
NV	1238.8210	< 16	< 13.06	< 13.06
OVI	1031.9261	71 ± 9	13.81 ± 0.06	13.7 ± 0.2
OVI	1037.6167	< 17	< 13.63	
SiIII	1206.5000	< 14	< 12.02	< 12.02

At $z = 0.09658$ we identify an absorber with similar characteristics to the O VI system at $z = 0.09180$. We measure a nearly identical O VI column density from the O VI 1031 profile but note the O VI 1037 transition is not detected at the 3σ level (Figure 5). We also caution that continuum placement is especially important for this absorber. Finally, one notes that the O VI 1031 profile extends to $v \approx -50\,\mathrm{km\ s}^{-1}$ whereas O VI 1037 is confined to $v > -20\,\mathrm{km\ s}^{-1}$ (in both the LiF2A and LiF1B channels). In any event, we adopt a final column density $N(\mathrm{O\,VI}) = 10^{13.7\pm0.2}\,\mathrm{cm}^{-2}$ based on the column densities of both profiles. For now, we include this absorber in our sample and note that FUSE Cycle 4 observations of PKS0405–123 (PI: Howk) should resolve these concerns. A curve-of-growth analysis shows this system has nearly the same N(HI) value as the $z = 0.09180$ absorber and a

comparable Doppler width $b = 40 \pm 2$ km s^{-1}.

Although the C III 977 transition is blended with a coincident transition, the absorption at $v \approx +10$ km s^{-1} is most likely related to this absorber and we report a value for its column density by integrating from $v \approx -10$ to $+20$ km s^{-1}. If the C III gas arises in the same ionization phase as the O VI gas, the absorber cannot be explained by a single-phase CIE model[6]. The collisional ionization models (Figure 2) do yield a solution with $\log N(\mathrm{C\,III})/N(\mathrm{O\,VI}) \approx -1$ at $T \approx 2 \times 10^5$ K, yet the model also predicts $\log N(\mathrm{C\,IV})/N(\mathrm{C\,III}) > 1$ in contradiction with the observations. Similarly, this model would predict a N V detection unless [N/O] < -0.8 dex. In contrast, a photoionization model with $\log U \approx -1.2$ matches the observed $N(\mathrm{C\,III})/N(\mathrm{O\,VI})$ ratio and also predicts C IV and N V column densities consistent with the observed upper limits (e.g. Figure 1). Therefore, we contend photoionization is the principal ionization mechanism for this system. Adopting $\log U = -1.2 \pm 0.2$, we estimate the gas metallicity [O/H] $= -1.5 \pm 0.3$ dex.

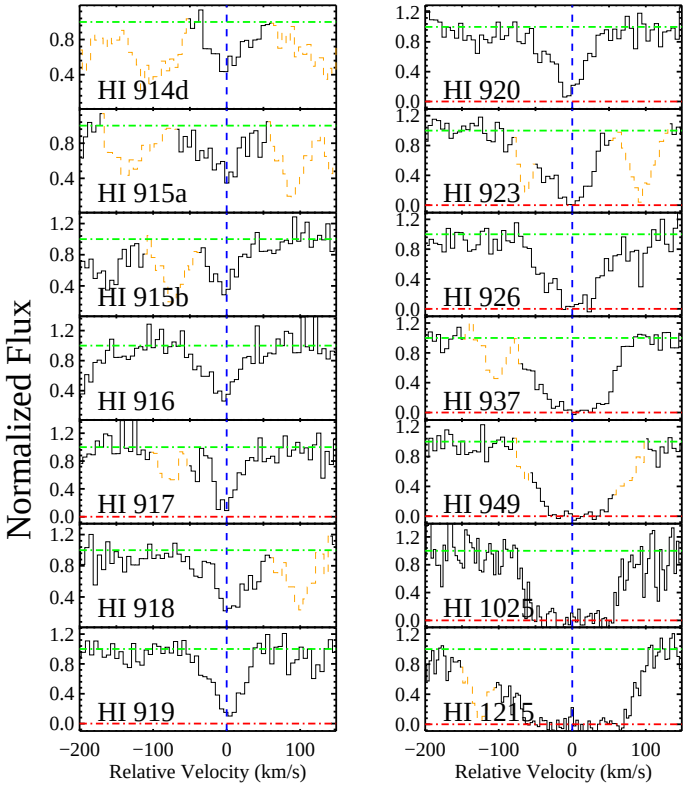

FIG. 6.— Velocity profiles of the Lyman series for the partial Lyman limit at $z = 0.16710$ toward PKS0405–123.

4.3. $z = 0.16710$

This absorption system was the principal motivation for the pursuit of FUSE observations of PKS0405–123. In particular, these data allow an analysis of the Lyman series (Figure 6) and therefore a determination of its N(HI) value. The absorber is a partial Lyman limit system, i.e., the optical depth at $\lambda_{rest} = 912$Å is $\tau_{912} \lesssim 1$. Therefore, one can independently solve for the total N(HI) value of this absorber through a COG analysis and a measurement of τ_{912}. The N(HI) value obtained from τ_{912} is not sensitive to the Doppler parameter, instrument line-spread function, or any component structure within the absorber. In short, the τ_{912} measurement tightly constrains the total HI column density with precision limited only by uncertainty in the quasar continuum. In Figure 7, we present the FUSE data covering the Lyman limit of the $z = 0.1671$

[6]If the absorption at $v < -20$ km s^{-1} in the O VI 1031 profile is confirmed in both O VI transitions (the current S/N is insufficient to make a definitive statement), then one may need to consider a multiphase or non-equilibrium model to explain the kinematic differences between the C III and O VI ions.

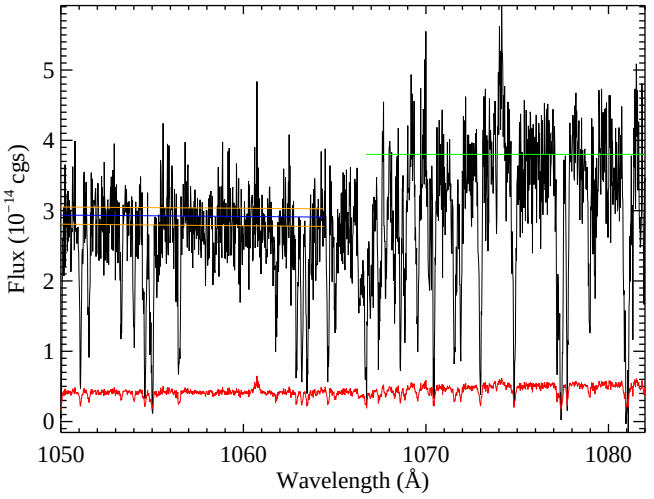

FIG. 7.— Lyman limit of the absorption system at $z = 0.16710$. The green line depicts our estimate of the flux redward of the Lyman limit and the blue line indicates our estimate of the flux blueward of the limit with a conservative error estimate (yellow lines). This flux decrement corresponds to $\log N(\mathrm{HI}) = 16.45 \pm 0.05$.

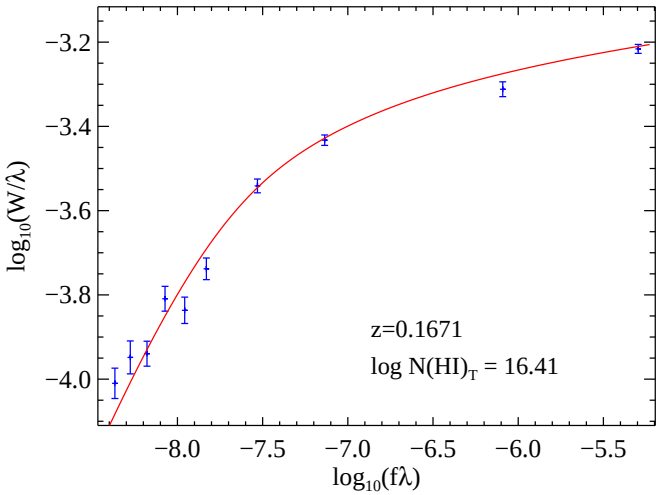

FIG. 8.— Curve-of-growth analysis of the Lyman series for the gas at $z = 0.16710$. In this analysis, we have assumed two components with $\log N(\mathrm{HI}) = 16.35$ and 15.5 and with 40 km s^{-1} separation.

system. The overplotted lines mark our assessment of the quasar continuum redward and blueward of $\lambda = 1066$Å. Even with a very conservative estimate of the continuum error, the uncertainty in N(HI) is $< 10\%$ and we find $N(\mathrm{HI}) = 10^{16.45\pm0.05}\,\mathrm{cm}^{-2}$.

Performing a COG analysis, we find that a single component model is a poor match to the observed W_λ values. Examining the low-ion profiles, we note that the C II and Si II profiles show two components at $v_1 \approx +5$ km s^{-1} and $v_2 \approx -35$ km s^{-1} in Figure 7. This suggests the H I profile is a combination of two components and that a two-component COG analysis is warranted. Indeed, a two component solution with $N_1(\mathrm{H\,I}) = 10^{16.35}\,\mathrm{cm}^{-2}$ and $N_2(\mathrm{H\,I}) = 10^{15.5}\,\mathrm{cm}^{-2}$ and component separation $\delta v = 40$ km s^{-1} is a good description of the EW observations (Figure 8). In the following analysis, we will not treat the components separately because (i) the N_2(H I) value is not well constrained and (ii) the components show similar relative ionic ratios (with the possible exception of N II).

The metal-line profiles for the low and high-ion species from the FUSE and STIS datasets are presented in Figures 9 and 10. The FUSE observations contribute a number of new metal transitions, although several of the most valuable profiles (e.g. O II 832, O III 834, N III 989) are unfortunately blended with strong Galactic transitions. The column density measurements and limits for all of the observed transitions are presented in Table 7. One notes that we report a 3σ detection for the O I 988 transition and a $> 2.5\sigma$ detection for the O I 1302 transition with consistent column densities. At present, we consider these tentative detections to be spurious primarily because the implied O metallicity is super-solar even prior to ionization corrections. Furthermore, the O I 1302 profile is more narrow than the other low-ion profiles and is offset from the O I 988 profile[7]. We hope that additional, planned FUSE observations of PKS0405–123 (PI: Howk) will confirm (or contradict) this tentative O I measurement. For now, we adopt an upper limit to $N(\mathrm{O}^0)$ of $10^{13.85}\,\mathrm{cm}^{-2}$.

Chen & Prochaska (2000) noted that no equilibrium photoionization or collisional ionization model could match the full set of ionic column densities measured for this absorber. In particular, the ionic column densities of the O VI and N V ions are too large to reconcile with the low and intermediate ions in a single ionization phase (e.g. consider Figures 1,2). This conclusion is supported by the differences between velocity centroids and Doppler widths measured for the N V and O VI profiles and those of the other metal-line profiles. Therefore, Chen & Prochaska (2000) analyzed the low and intermediate ions independent of the O VI and N V gas and we follow this approach. Specifically, we examine the ionization state required to give the N(O VI)/N(N V) ratio and independently the physical conditions that yield the lower ions.

Consider first the high-ions under the premise of collisional ionization. To reproduce the N(O VI)/N(N V) ratio with solar relative abundances, this implies $T \approx 2.5 \times 10^5$ K. At this temperature, this CIE phase would have a relatively small ionic column density for all other ions except C IV and S VI. The CIE model does predict $\log N(\mathrm{S\,VI}) = 12.9$ which matches the column density de-

[7]The latter effect could be a small calibration error

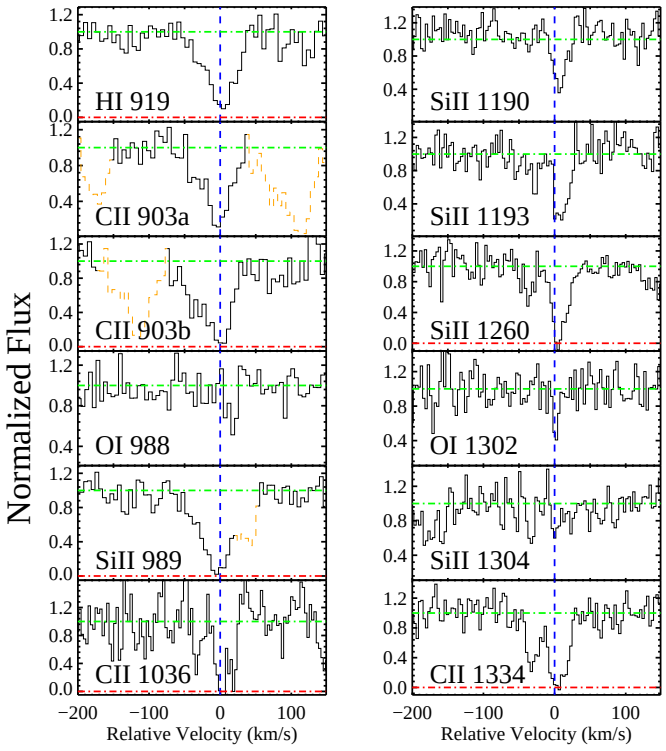

FIG. 9.— Velocity profiles of the low-ion metal transitions for the partial Lyman limit at $z = 0.16710$ toward PKS0405–123.

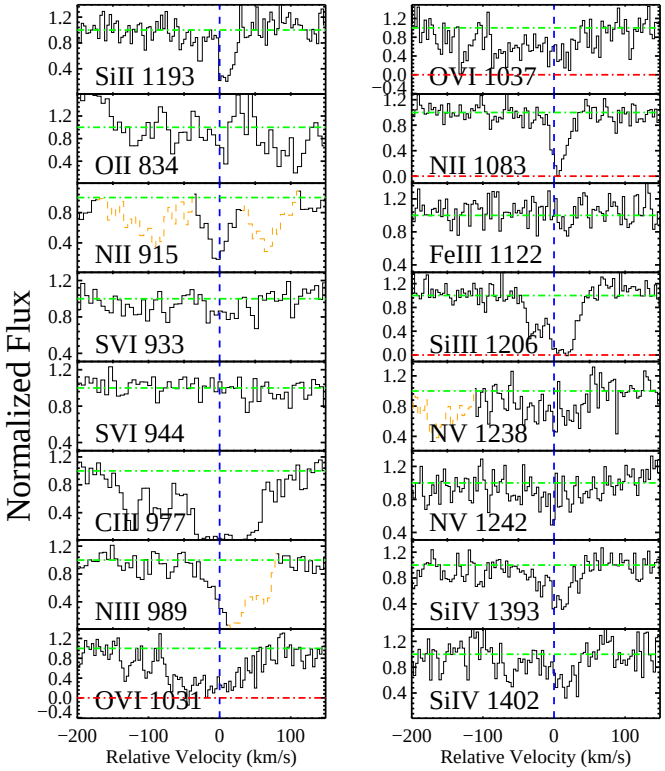

FIG. 10.— Velocity profiles of the intermediate and high-ion metal transitions for the partial Lyman limit at $z = 0.16710$ toward PKS0405–123.

TABLE 7
IONIC COLUMN DENSITIES FOR THE ABSORBER AT z=0.16710

Ion	λ (Å)	EW (mÅ)	AODM	N_{adopt}
HI				16.45 ± 0.07
CII	903.6240	125 ± 8	> 14.24	> 14.35
CII	903.9620	158 ± 8	> 14.13	
CII	1334.5323	197 ± 14	> 14.35	
CIII	977.0200	374 ± 8	> 14.27	> 14.27
NII	915.6130	104 ± 7	> 14.17	> 14.24
NII	1083.9900	93 ± 9	> 14.24	
NIII	989.7990	< 15	< 14.59	< 14.59
NV	1238.8210	114 ± 20	13.84 ± 0.07	13.89 ± 0.05
NV	1242.8040	78 ± 13	13.95 ± 0.07	
OI	988.7730	20 ± 6	13.84 ± 0.11	< 13.85
OI	1302.1685	30 ± 10	13.74 ± 0.14	
OII	834.4655	< 20	< 13.65	< 13.65
OVI	1031.9261	377 ± 20	> 14.74	14.78 ± 0.07
OVI	1037.6167	240 ± 23	14.78 ± 0.07	
SiII	1190.4158	26 ± 7	13.15 ± 0.09	13.30 ± 0.04
SiII	1193.2897	105 ± 11	13.42 ± 0.05	
SiII	1260.4221	140 ± 11	> 13.36	
SiII	1304.3702	19 ± 6	13.23 ± 0.14	
SiIII	1206.5000	204 ± 10	> 13.39	> 13.39
SiIV	1393.7550	140 ± 14	13.33 ± 0.04	13.34 ± 0.04
SiIV	1402.7700	92 ± 16	13.44 ± 0.08	
SIII	1190.2080	< 13	< 13.83	< 13.83
SIV	809.6680	< 22	< 13.80	< 13.80
SIV	1062.6620	< 18	< 13.89	
SVI	933.3780	24 ± 8	12.91 ± 0.13	12.91 ± 0.13
SVI	944.5230	< 11	< 12.95	
FeII	1144.9379	< 9	< 13.15	< 13.15
FeIII	1122.5260	< 16	< 13.60	< 13.60

rived from S VI λ933, although this measurement has a large uncertainty. Future observations of C IV $\lambda\lambda$1548, 1550 and S VI would verify the assumption of CIE and tightly constrain the temperature of this phase. In passing, we note that the metallicity of the gas assuming $T = 2.5 \times 10^5$ K and $N(\mathrm{HI}) = 10^{16}\,\mathrm{cm}^{-2}$ is [O/H] ≈ -1 dex.

We now focus on the lower ionization phase which we expect is predominantly photoionized. Figure 11 presents the predicted ionic column densities for a range of ions assuming a plane-parallel slab of gas with $N(\mathrm{HI}) = 10^{16.5}\,\mathrm{cm}^{-2}$, metallicity [M/H] $= -0.25$ dex, and the EUVB model Q at $z = 0.2$ (see § 3). Comparisons of the model predictions with the observed ionic ratios constrain the ionization parameter and provide estimates to the ionization corrections. The tightest constraints on the ionization parameter comes from the Si and N ions. The $N(\mathrm{Si\,II})/N(\mathrm{Si\,III})$, $N(\mathrm{N\,II})/N(\mathrm{N\,III})$, $N(\mathrm{Si\,II})/N(\mathrm{Si\,IV})$ limits and the $N(\mathrm{Si\,II})/N(\mathrm{Si\,IV})$ measurement imply the dashed (lower limits), dotted (upper limits), and dash-dot (measurements) lines overplotted on Figure 11. Formally, no single ionization parameter satisfies all of the constraints. Given that the Cloudy calculations are based on simplified assumptions (e.g. constant density, single temperature), the results are in good agreement[8] with $\log U = -2.9 \pm 0.2$ dex. Applying the appropriate ionization corrections, we find [Si/H] $\approx -0.25 \pm 0.2$ dex based on the $N(\mathrm{Si\,II})/N(\mathrm{HI})$ ratio which is relatively insensitive to U at these values. We adopt a conservative error on [Si/H] reflecting the systematic uncertainties of photoionization modeling. One may formally refer to this metallicity as a lower limit because an unknown fraction of H I gas must be attributed to the more highly ionized gas phase. We suspect, however, that this would imply at most a 0.3 dex increase in [Si/H].

[8] It is worth noting that adopting a softer ionizing spectrum (e.g. Model QG) would worsen the disagreement between the N and Si ions.

TABLE 8
ELEMENTAL ABUNDANCES FOR THE ABSORBER AT z=0.16710

Ion	[X/H]	[X/Si$^+$]
C^+	> -0.32	> -0.03
C^{++}	> -0.88	> -0.59
N^+	> 0.19	> 0.48
N^{++}	< 0.07	< 0.35
N^{+4}	1.86 ± 0.30	2.15
O^0	< 1.13	< 1.41
O^+	< -1.33	< -1.04
O^{+5}	3.88 ± 0.49	4.17
Si^+	-0.29 ± 0.02	0.00
Si^{++}	> -0.65	> -0.36
Si^{+3}	-0.04 ± 0.20	0.25
S^{++}	< 0.07	< 0.36
S^{+3}	< 0.95	< 1.23
S^{+5}	1.34 ± 0.37	1.63
Fe^+	< 0.78	< 1.06
Fe^{++}	< -0.14	< 0.15

Table 8 lists the [X/H] and [X/Si$^+$] values for all of the ions observed in this partial LLS assuming $U_{best} = 10^{-3.0 \pm 0.1}$. For illustration, we include N V and O VI to demonstrate these ions cannot be in photoionization equilibrium with the other ions because one predicts very low values compared to the observations. For S and Fe (marked by non-detections), the calculated upper limits on [S/H]

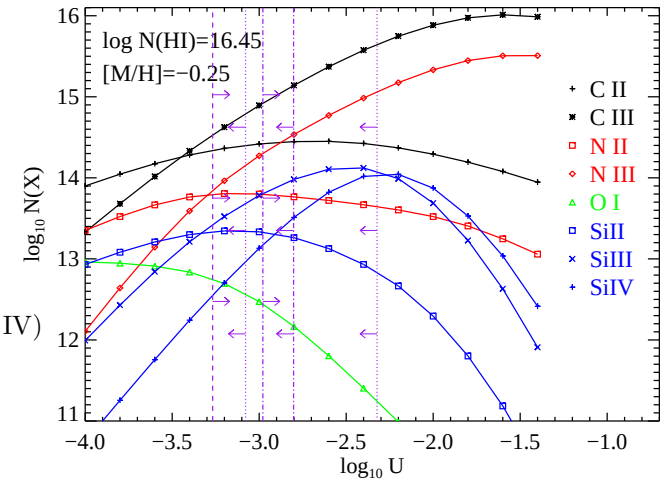

FIG. 11.— Predicted ionic column densities for the absorber at $z = 0.16710$ assuming photoionization and a quasar-only extragalactic UV background (model Q) at $z = 0.15$, a total H I column density $N(\mathrm{HI}) = 10^{16.45}\,\mathrm{cm}^{-2}$, and solar relative abundances scaled to a metallicity [M/H] $= -0.25$ dex. The purple dashed line shows a lower limit to U based on the $N(\mathrm{Si\,II})/N(\mathrm{Si\,III})$ upper limit whereas the dotted purple lines show upper limits to U based on limits to the $N(\mathrm{N\,II})/N(\mathrm{N\,III})$ and $N(\mathrm{Si\,II})/N(\mathrm{Si\,IV})$ ratios. Finally the $N(\mathrm{Si\,II})/N(\mathrm{Si\,IV})$ value and 1σ error constrain U to the region indicated by the dash-dot purple lines.

and [Fe/H] are consistent with expectation. The C ions are also in reasonable agreement although the lower limits from C II nearly conflict with the Si abundance under the presumption of solar relative abundances. As noted above, if the O I transitions are true detections they imply a large O abundance and a correspondingly large O/Si ratio. If future observations yield an $N(O^0)$ value near our upper limit, the super-solar O/Si ratios might indicate gas enriched by massive ($M > 15 M_\odot$) Type II SN (Woosley & Weaver 1995).

Because the FUSE+STIS datasets provide full coverage of the dominant Si and N ions indicated by the photoionization modeling, it is possible to calculate the N/Si ratio largely independent of ionization corrections for the photoionized gas[9]:

$$\frac{\mathrm{N}}{\mathrm{Si}} = \frac{N(\mathrm{N\,II}) + N(\mathrm{N\,III})}{N(\mathrm{Si\,II}) + N(\mathrm{Si\,III}) + N(\mathrm{Si\,IV})} \quad . \qquad (1)$$

Summing over the column densities and assuming reasonable values for the limits, we find $\log(\mathrm{N/Si}) \gtrsim +0.5$ or $[\mathrm{N/Si}] \gtrsim +0.2$ dex. We derive a similar value by considering only the $N(\mathrm{N\,II})/N(\mathrm{Si\,II})$ ratio which has a small dependence on U for $\log U < -2.7$ dex. This N/Si overabundance is a surprising result; there are few examples of enhanced N abundances in the local universe. We also note that the O and C observations are consistent with enhancements of these elements relative to Si suggesting an overabundance of all the light elements. One of the few sites where large N abundances are observed are quasars (Osmer 1980; Bentz, Hall, & Osmer 2004). Given the properties of high metallicity, enhanced light elements, and substantial separation from any bright galaxy (Prochaska et al. 2004), one may speculate that this gas was related to AGN activity.

4.4. $z = 0.18250$ *and* $z = 0.18290$

The system at $z = 0.183$ is notable for showing large $N(\mathrm{O\,VI})/N(\mathrm{HI})$ variations in a pair of absorbers separated by $\delta v < 100$ km s^{-1} . Figure 12 plots the H I and metal-line profiles for the two absorbers with $z = 0.18250$ ($v = -25$ km s^{-1}) and $z = 0.18290$ ($v = +50$ km s^{-1}). We performed separate COG analyses and derived H I column densities $N(\mathrm{HI}) = 10^{14.50\pm0.05}$ cm^{-2} and $10^{14.08\pm0.1}$ cm^{-2} and Doppler parameters $b = 27 \pm 1$ km s^{-1} and $b = 26 \pm 5$ km s^{-1} respectively. The only metal-line absorption that we confidently identify with this system is O VI gas related to the $z = 0.1829$ absorber. There is a hint of O VI absorption at the velocity corresponding to the $z = 0.1825$ absorber, but the measured equivalent width is less than a 3σ detection. At this redshift, the FUSE data provide coverage of the O III 832 and O IV 787 transitions of this absorber. Unfortunately, the O IV 787 transition is significantly blended with an H_2 transition. The O III 832 region is also partially contaminated but provides a meaningful upper limit on the O III column density (Tables 9, 10).

We detect no other ions for these two absorbers. Most importantly, we place an upper limit to $N(\mathrm{C\,III}) < 10^{12.4}$ cm^{-2} for the absorber at $z = 0.18290$ [10]. If the gas is photoion-

[9]Note $N(\mathrm{N\,IV})$ and $N(\mathrm{N\,V})$ are assumed to be smaller than the upper limit obtained for $N(\mathrm{N\,III})$

[10]The C III 977 profile is blended with an H_2 transition at the velocity corresponding to $z = 0.18250$.

TABLE 9
IONIC COLUMN DENSITIES FOR THE ABSORBER AT z=0.18250

Ion	λ (Å)	EW (mÅ)	AODM	N_{adopt}
HI				14.90 ± 0.05
NV	1238.8210	< 14	< 12.99	< 12.99
OII	834.4655	< 21	< 14.55	< 14.55
OIII	832.9270	< 18	< 13.73	< 13.73
OIV	787.7110	< 19	< 13.83	< 13.83
OVI	1031.9261	< 28	< 13.77	< 13.77
OVI	1037.6167	< 23	< 13.95	
SiII	1260.4221	< 15	< 12.21	< 12.21
SiIII	1206.5000	< 14	< 11.99	< 11.99
SiIV	1393.7550	< 28	< 12.64	< 12.64

TABLE 10
IONIC COLUMN DENSITIES FOR THE ABSORBER AT z=0.18290

Ion	λ (Å)	EW (mÅ)	AODM	N_{adopt}
HI				14.08 ± 0.10
CIII	977.0200	< 11	< 12.42	< 12.42
NV	1238.8210	< 15	< 13.05	< 13.05
OIII	832.9270	< 25	< 13.79	< 13.79
OIV	787.7110	< 22	< 14.61	< 14.61
OVI	1031.9261	72 ± 18	13.94 ± 0.12	13.96 ± 0.07
OVI	1037.6167	44 ± 9	13.97 ± 0.09	
SiIII	1206.5000	< 14	< 12.01	< 12.01
SiIV	1393.7550	< 27	< 12.68	< 12.68

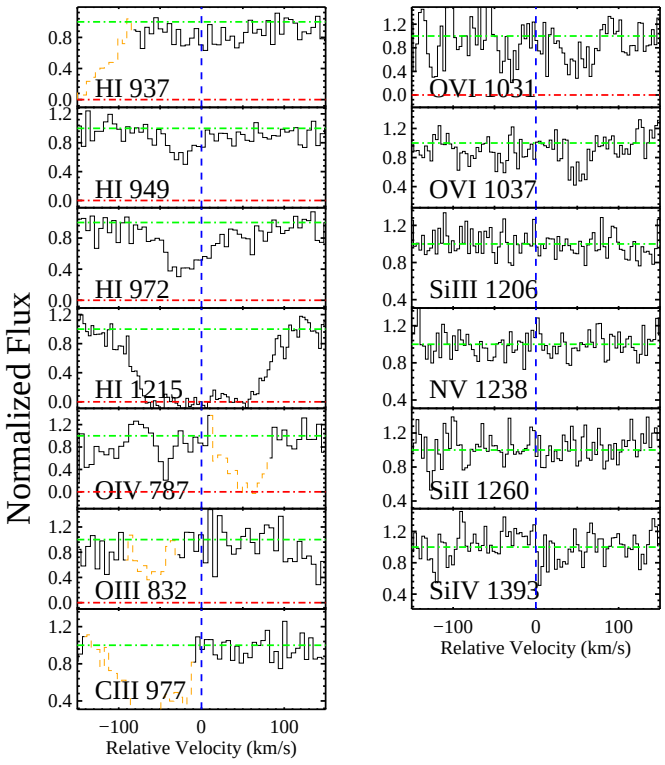

FIG. 12.— Velocity profiles of the Lyman series and metal-line transitions analyzed for the pair of absorption systems at $z = 0.183$. The dotted line in the figure corresponds to $z = 0.18270$.

ized, the $N(\mathrm{O\,VI})/N(\mathrm{C\,III})$ ratio requires an ionization parameter $\log U > -1$ for solar relative abundances which implies $[\mathrm{O/H}] > -1$ (e.g. Figure 1). Under the assumption of collisional ionization, however, the $N(\mathrm{C\,III})/N(\mathrm{O\,VI})$ limit requires $T > 2 \times 10^5$ K and suggests metallicity $-2 < [\mathrm{O/H}] < -1$. If we ignore the Doppler parameter of the H I gas which is uncertain, both solutions are allowed but imply temperatures for the gas which differs by more than one order of magnitude. A detection or sensitive limit to the $N(\mathrm{C\,IV})$ value would likely resolve the degeneracy; this measurement could be achieved with future HST+STIS observations of PKS0405–123.

Irrespective of the ionization mechanism, the absorbers are notable for exhibiting $N(\mathrm{O\,VI})/N(\mathrm{HI})$ ratios differing by more than an order of magnitude in gas separated by $\delta v < 100\,\mathrm{km\,s^{-1}}$ (see also Savage et al. 2002). Under the assumption of photoionization, the variation in $N(\mathrm{O\,VI})/N(\mathrm{HI})$ can only be explained through large differences in [M/H] and/or n_H. For example, the $z = 0.18250$ absorber may have substantially higher gas density and a correspondingly lower ionization parameter. In this case, however, the models predict $N(\mathrm{O\,IV})$ values inconsistent with the observed upper limits. Therefore, if the gas is photoionized the absorber at $z = 0.18290$ has at least 10× higher metallicity. This would indicate a remarkable level of inhomogeneity in metal enrichment and would be particularly surprising given the $z = 0.18290$ absorber has lower H I column density. If collisional ionization is the dominant mechanism, then the $N(\mathrm{O\,VI})/N(\mathrm{HI})$ ratios imply large temperature differences if the two absorbers have comparable metallicity (e.g. $T \gtrsim 10^6$K for the gas at $z = 0.18250$ and $T \approx 3 \times 10^5$K for the gas at $z = 0.18290$). If we require $T > 2 \times 10^5$ K for the $z = 0.18290$ system based on the non-detection of C III, then we derive a temperature for the $z = 0.18250$ absorber which is inconsistent at greater than 5σ significance from the COG analysis. Therefore, it is likely that a CIE model would also require a large (> 0.3 dex) difference in [O/H].

4.5. $z = 0.36080$

There is a complex, highly ionized absorption system at $z = 0.36080$ toward PKS0405–123. The FUSE+STIS datasets show Lyα-Ly6 absorption (Figure 13) which shows a hint of two closely separated components. A single component COG analysis, however, provides a good description of the data and reveals $N(\mathrm{HI}) = 10^{15.12\pm0.05}\,\mathrm{cm^{-2}}$ and $b = 27 \pm 1\,\mathrm{km\,s^{-1}}$. We identify a series of metal-line transitions including absorption from O III O IV, and C III (Figure 14, Table 11). We also detect N IV 765 and Si III 1206 but report upper limits because of line blending. Finally, there is a 2σ detection of the N III 989 transition and a feature at the expected position of N V 1238. We suspect the latter feature is related to fixed pattern noise or detector artifact because the observed optical depth is only marginally consistent with the null detection of N V 1242 and because of the implied N abundance: [N/Si] > 0.5 dex. Interestingly, this absorber shows no low-ion gas and also no O VI absorption. We predict the absorber will show significant C IV absorption and, therefore, may be an analog to high z C IV systems with comparable H I column density (e.g. Sargent, Steidel, & Boksenberg 1988). Indeed, this is apparently the case as Williger et al. (2004)

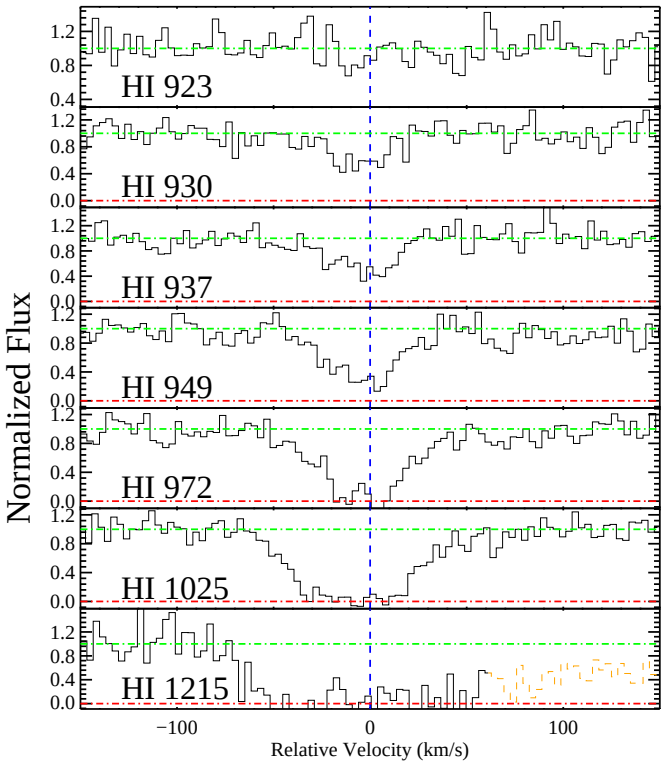

FIG. 13.— Velocity profiles of the Lyman series for the absorption system at $z = 0.36080$ toward PKS0405–123.

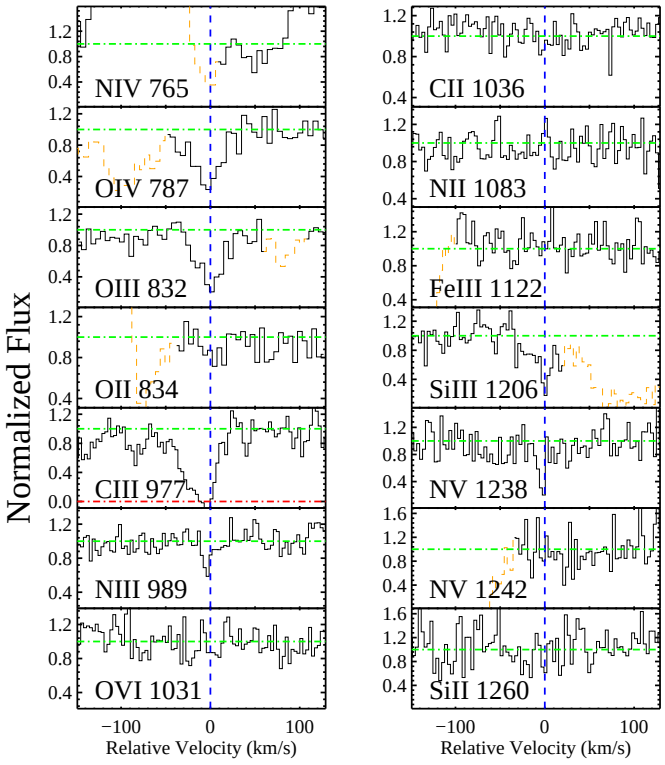

FIG. 14.— Velocity profiles of the metal-line transitions for the absorption system at $z = 0.36080$.

find $\log N(\mathrm{CIV}) = 13.76 \pm 0.16$ based on their analysis of STIS G230M archival data.

TABLE 11
IONIC COLUMN DENSITIES FOR THE ABSORBER AT z=0.36080

Ion	λ (Å)	EW (mÅ)	AODM	N_{adopt}
HI				15.12 ± 0.05
CII	1036.3367	< 13	< 13.21	< 13.21
CIII	977.0200	152 ± 7	> 13.78	> 13.78
NII	1083.9900	< 19	< 13.47	< 13.47
NIII	989.7990	< 11	< 13.31	< 13.31
NIV	765.1480	< 8	< 13.22	< 13.22
NV	1238.8210	< 23	< 13.52	< 13.52
NV	1242.8040	< 32	< 13.75	
OII	834.4655	< 10	< 13.25	< 13.25
OIII	832.9270	72 ± 5	> 14.17	> 14.17
OIV	787.7110	75 ± 7	> 14.26	> 14.26
OVI	1031.9261	< 16	< 13.30	< 13.30
SiII	1260.4221	< 28	< 12.55	< 12.55
SiIII	1206.5000	< 19	< 12.64	< 12.64
FeIII	1122.5260	< 19	< 13.67	< 13.67

Examining the collisional ionization solutions described by Figure 2, a solution with $T \approx 1.3 \times 10^5$ K matches the relative column densities of the O ions. We do not favor this scenario, however, for several reasons. First, collisional ionization implies $N(\mathrm{C\,III})/N(\mathrm{O\,III}) \approx -0.8$ yet we observe $N(\mathrm{C\,III})/N(\mathrm{O\,III}) > -0.4$ under the assumption that the C III 977 profile requires larger corrections for line-saturation than O III 832. Second, the temperature is inconsistent at $> 5\sigma$ with the value implied by the measured H I Doppler parameter. Third, the predicted $N(\mathrm{N\,III})/N(\mathrm{N\,IV})$ ratio is only marginally consistent with the observed limits. Although none of these arguments is decisive, together they imply collisional ionization is not the dominant ionization process. A conclusive test (e.g. observations of the C IV doublet) would be valuable as CIE models imply significantly lower metallicity and correspondingly higher N(H) than photoionization.

Assuming photoionization, the measurements and limits on the column densities of the O ions tightly constrain the ionization state of this gas (Figure 15). Treating the O III and O IV column densities as lower limits because of line saturation, the resulting $N(\mathrm{O\,II})/N(\mathrm{O\,IV})$ and $N(\mathrm{O\,III})/N(\mathrm{O\,VI})$ limits require $-2.1 < \log U < -1.7$. If we adopt $\log[N(\mathrm{O\,III})/N(\mathrm{O\,IV})] = 0.1 \pm 0.2$, this places a similar constraint on the U parameter. In Table 12, we list the ions analyzed for this absorber and [X/H] values corresponding to $U_{best} = 10^{-1.9 \pm 0.2}$. The principal result is that the lower limits to O III and O IV imply $[\mathrm{O/H}] \gtrsim -0.7$, an enrichment level consistent with the lower limit to the C III column density.

Because the ionization corrections for O III/C III are nearly constant at -0.2 dex for the relevant ionization parameter, we estimate $[\mathrm{O/C}] \lesssim +0.2$ based on the saturated O III λ832 and C III λ977 profiles. In this absorber, at least, it is unlikely the gas has a super-solar O/C ratio, in contrast to the abundances inferred for a sample of $z \gtrsim 1$ absorption systems with comparable ionization state (Vogel & Reimers 1995). The upper limit measurements for the nitrogen ions also place a limit on the N/O abundance. In particular, note that the predicted N III column density closely traces $N(\mathrm{O\,III})$ for $\log U \approx -2$. Therefore, the ratio of these ions provides a measurement of N/O largely independent of uncertainties in the ionization parameter: $[\mathrm{N/O}] < -0.2$ dex. Noting that the $N(\mathrm{N\,III})$ value is likely to be within ≈ 0.1 dex of the adopted upper limit (weak absorption is apparent at the expected position of N III 989), we report $[\mathrm{N/O}] = -0.3 \pm 0.15$ dex. This relative abundance follows the [N/O] vs. [O/H] trend observed for galaxies in the local universe (e.g. Henry, Edmunds, & Köppen 2000).

TABLE 12
ELEMENTAL ABUNDANCES FOR THE ABSORBER AT z=0.36080

Ion	[X/H]	[X/Si$^+$]
C^+	< 0.03	< 0.78
C^{++}	> -1.05	> -0.30
N^+	< 1.08	< 1.83
N^{++}	< -0.96	< -0.21
N^{+3}	< -0.92	< -0.17
N^{+4}	< -0.07	< 0.68
O^+	< 0.15	< 0.90
O^{++}	> -0.75	> 0.00
O^{+3}	> -0.76	> -0.01
O^{+5}	< -0.54	< 0.20
Si^+	< 1.34	< 2.09
Si^{++}	< 0.12	< 0.87
Fe^{++}	< 3.77	< 4.52

Because this absorber is characterized by higher ionization states, the results are sensitive to the assumed shape of the EUVB radiation field. If we adopt the softer model QG, the observed ionic ratios for oxygen require a higher ionization parameter ($U \approx -1.4$) and imply lower

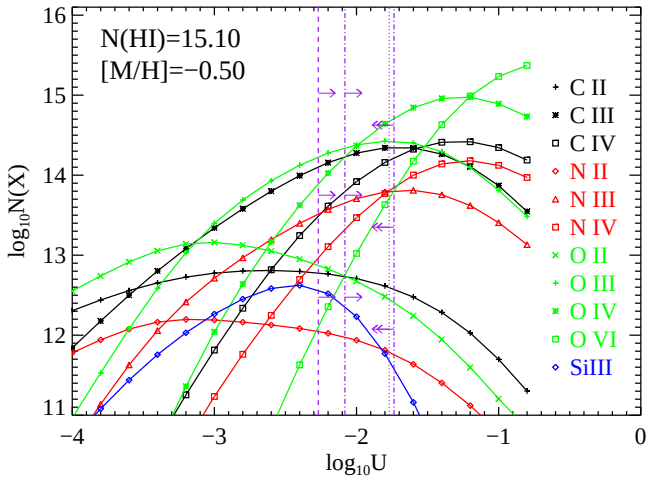

FIG. 15.— Predicted ionic column densities for the absorber at $z = 0.36080$ assuming photoionization and a quasar-only extragalactic UV background (model Q) at $z = 0.35$, a total H I column density $N(\mathrm{HI}) = 10^{15.10}\,\mathrm{cm}^{-2}$, and solar relative abundances scaled to a metallicity $[\mathrm{M/H}] = -0.50$ dex. The purple dashed line shows a lower limit to U based on the $N(\mathrm{O\,II})/N(\mathrm{O\,IV})$ upper limit whereas the dotted purple line shows an upper limits to U based on the lower limit to $N(\mathrm{O\,IV})/N(\mathrm{O\,VI})$. Finally the $N(\mathrm{O\,III})/N(\mathrm{O\,IV})$ value and 1σ error constrain U to the region indicated by the dash-dot purple lines.

elemental abundances ([O/H] > -1.2). The latter result is a consequence of the higher H ionization fraction of the softer spectrum. Again, a measurement of the C IV column density would help resolve this ambiguity. Additionally, tighter constraints on the column densities of O VI and the N ions would probe the shape of the ionizing spectrum.

TABLE 13
IONIC COLUMN DENSITIES FOR THE ABSORBER AT z=0.36332

Ion	λ (Å)	EW (mÅ)	AODM	N_{adopt}
HI				13.43 ± 0.10
CII	1036.3367	< 13	< 13.22	< 13.22
CIII	977.0200	22 ± 7	12.64 ± 0.12	12.64 ± 0.12
NII	1083.9900	< 15	< 13.33	< 13.33
NIII	989.7990	< 19	< 13.47	< 13.47
NIV	765.1480	42 ± 7	> 13.22	> 13.22
NV	1238.8210	< 27	< 13.34	< 13.35
NV	1242.8040	< 31	< 13.70	
OII	834.4655	< 13	< 13.33	< 13.33
OIII	832.9270	< 11	< 13.40	< 13.40
OIV	787.7110	28 ± 6	13.73 ± 0.10	13.73 ± 0.10
OVI	1031.9261	23 ± 8	13.44 ± 0.11	13.44 ± 0.11
OVI	1037.6167	< 11	< 13.45	
NeVIII	770.4090	< 13	< 13.55	< 13.55
SiII	1260.4221	< 31	< 12.53	< 12.53
SiIII	1206.5000	< 24	< 12.26	< 12.26

4.6. $z = 0.36332$

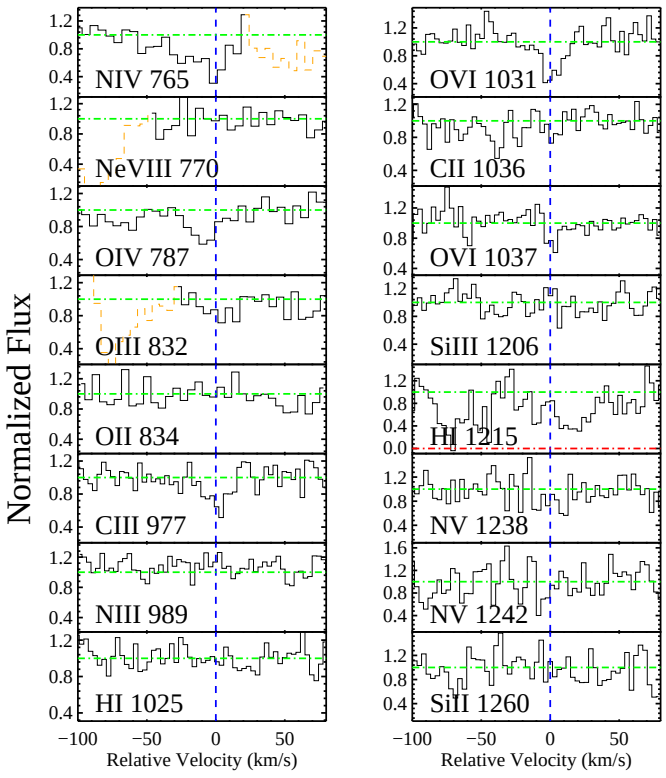

FIG. 16.— Velocity profiles of the Lyman series and metal-line transitions analyzed for the absorption system at $z = 0.36332$.

There is a neighboring absorber (at $+550\,\mathrm{km\,s^{-1}}$) to the $z = 0.36080$ system which shows O IV, O VI, N IV, and C III absorption yet a weak and unusual Lyα profile (Figure 16). In particular, one notes that the metal-lines are significantly offset from the H I absorption. Integrating the Lyα profile from $v = -30$ to $+80\,\mathrm{km\,s^{-1}}$, we derive an H I column density $N(\mathrm{HI}) = 10^{13.4\pm0.2}\,\mathrm{cm^{-2}}$. In the following, we will adopt this value but one may consider it an upper limit to the H I column density associated with this metal-line system. It would be extremely valuable to have higher S/N of the C IV and Lyα spectral regions for this absorber to more confidently compare their line profiles. We suggest this system is an example of an O VI absorber without detected neutral hydrogen gas which implies a very high temperature and/or metallicity. Table 13 lists the ionic column densities for this absorber which includes an upper limit on N(N IV) based on the blended N IV 765 profile.

TABLE 14
ELEMENTAL ABUNDANCES FOR THE ABSORBER AT z=0.36332

Ion	[X/H]	[X/Si$^+$]
C^+	< 2.36	< 2.34
C^{++}	-0.37 ± 0.10	-0.39
N^+	< 3.22	< 3.20
N^{++}	< 0.97	< 0.95
N^{+3}	> 0.34	> 0.32
N^{+4}	< 0.58	< 0.56
O^+	< 2.59	< 2.57
O^{++}	< 0.31	< 0.29
O^{+3}	0.02 ± 0.07	0.00
O^{+5}	0.04 ± 0.44	0.02
Ne^{+7}	< 0.05	< 0.03
Si^+	< 4.79	< 4.77
Si^{++}	< 2.92	< 2.90

It is surprising, however, that the absorber also shows C III 977. Regarding collisional ionization equilibrium models, there is no single temperature solution which would give $N(\mathrm{C\,III})/N(\mathrm{O\,VI}) \approx 0.15$ ($T < 2 \times 10^5\,\mathrm{K}$) and $N(\mathrm{O\,IV})/N(\mathrm{O\,VI}) \approx 2$ ($T \approx 2.5 \times 10^5\,\mathrm{K}$) assuming solar relative abundances. Although the difference in these temperatures may appear small, the relative abundances of $N(\mathrm{C\,III})/N(\mathrm{O\,VI})$ and $N(\mathrm{O\,IV})/N(\mathrm{O\,VI})$ are very sensitive to temperature (see also Howk et al. 2004). For example, assuming $T = 2.5 \times 10^5$K would underpredict [C/O] by two orders of magnitude. Therefore, a single-phase CIE model cannot fully describe this absorber. Adopting photoionization as the dominant mechanism, the best model has $\log U = -1.4 \pm 0.2$ assuming the EUVB model Q and [M/H] =0. Table 14 presents the [X/H] and [X/O^{+3}] values for $U_{best} = 10^{-1.4\pm0.2}$. Even adopting $N(\mathrm{HI}) = 10^{13.4}\,\mathrm{cm^{-2}}$, we calculate a solar oxygen abundance for this absorber. Independent of the N(HI) value we find [O/C] $\approx +0.4 \pm 0.2$ dex. These abundances are comparable to those derived from the nearby $z = 0.36080$ system. Although the velocity separation is too large to associate spatially the gas, the 'clouds' may have a common enrichment history suggesting a similar physical origin.

TABLE 15
IONIC COLUMN DENSITIES FOR THE ABSORBER AT z=0.49510

Ion	λ (Å)	EW (mÅ)	AODM	N_{adopt}
HI				14.39 ± 0.07
CII	903.9616	< 20	< 13.08	< 13.08
CIII	977.0200	61 ± 7	13.18 ± 0.06	13.18 ± 0.06
NII	1083.9900	< 22	< 13.47	< 13.47
NIII	989.7990	< 12	< 13.29	< 13.29
NIV	765.1480	< 16	< 12.88	< 12.88
OII	834.4655	< 13	< 13.37	< 13.37
OIII	832.9270	< 15	< 13.59	< 13.59
OIV	787.7110	105 ± 9	> 14.34	> 14.34
OV	629.7300	164 ± 9	> 14.41	> 14.41
OVI	1031.9261	133 ± 9	14.25 ± 0.04	14.26 ± 0.03
OVI	1037.6167	94 ± 10	14.31 ± 0.06	
NeVIII	770.4090	26 ± 7	13.75 ± 0.10	13.75 ± 0.10
NeVIII	780.3240	< 14	< 13.86	
MgX	624.9500	< 16	< 14.22	< 14.22
SVI	933.3780	< 9	< 12.62	< 12.62

4.7. $z = 0.4951$

The highest redshift metal-line system along the sightline to PKS0405–123 is at $z = 0.495$ and exhibits detections of C III, O IV, O V, and possibly Ne VIII transitions. Williger et al. (2004) performed a profile fit to the Lyβ transition and measured $\log N(\mathrm{HI}) = 14.39 \pm 0.07$ and $b = 60 \pm 15$ km s^{-1} consistent with our W$_\lambda$ measurements. The H I and metal-line profiles are presented in Figure 17 and the ionic column densities are listed in Table 15.

A full analysis of this absorber is presented in Howk et al. (2004) and we only summarize a few key results here. The FUSE spectra provide constraints on a number of transitions which are very rarely observed in intervening quasar absorption line systems including O V 629, N IV 765, and the Ne VIII and Mg X doublets. Altogether, the FUSE+STIS datasets provide a comprehensive analysis of the ionization state of this gas. While a collisional ionization model with $T \approx 2.3 \times 10^5$ K can reproduce the observed O ionic column densities, this model underpredicts N(C III) by over 2 orders of magnitude. Therefore, Howk et al. (2004) rule out a single-phase CIE model. In contrast, the gas is well modeled by a single-phase photoionization model with $\log U \approx -1.2$ although a two-phase model (collisional plus photoionization) is also allowed. We summarize the physical properties of this gas in the following section.

5. $N(\mathrm{HI}) > 10^{14}\,\mathrm{cm}^{-2}$ ABSORBERS WITHOUT METAL-LINE TRANSITIONS

In our analysis of PKS0405–123 we have searched for metal-line transitions in every Lyα absorption system identified by Williger et al. (2004), with special attention to $N(\mathrm{HI}) > 10^{14}\,\mathrm{cm}^{-2}$ systems. This allows us to investigate the metallicity distribution of a 'complete' sample of low redshift, $N(\mathrm{HI}) > 10^{14}\,\mathrm{cm}^{-2}$ Lyα clouds. Perhaps the most remarkable example is the absorber at $z = 0.40570$. Although this absorber shows nearly the same H I column density as the metal-line system at $z = 0.36080$, it is remarkable for exhibiting no metal-line transitions. In Figure 18 we present the Lyman series and a set of the strongest metal transitions covered by the FUSE and

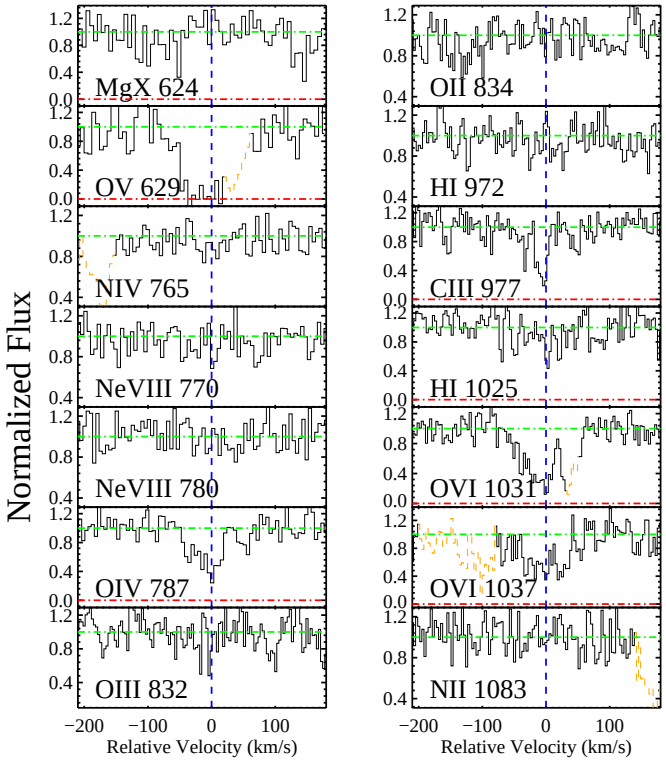

FIG. 17.— Velocity profiles of the Lyman series and metal-line transitions analyzed for the absorption system at $z = 0.49510$.

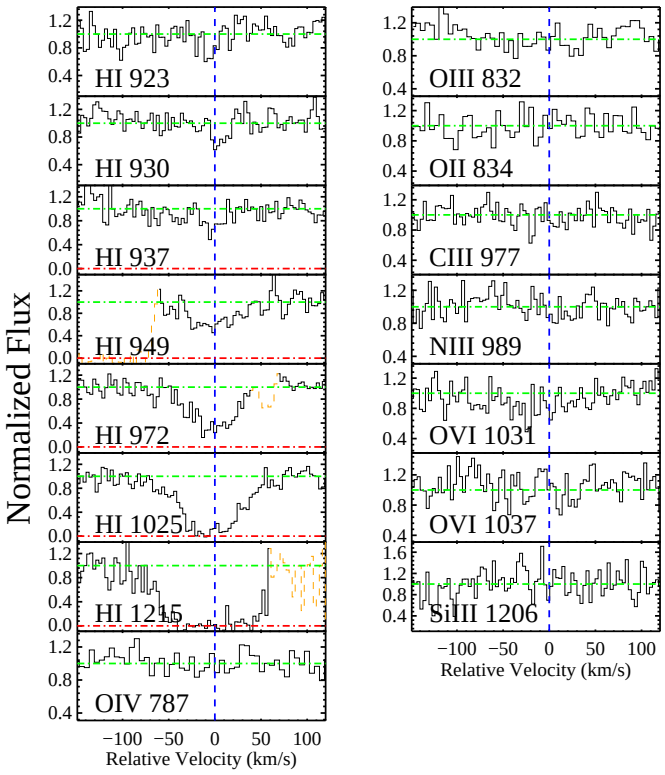

FIG. 18.— Velocity profiles of the Lyman series and metal-line transitions analyzed for the absorption system at $z = 0.40570$. Note that none of the metal-line transitions show significant detections.

STIS spectra (Table 16). A COG analysis gives $N(\mathrm{HI}) = 10^{14.85\pm0.05}\,\mathrm{cm}^{-2}$ with Doppler parameter $b = 34\pm2$ km s^{-1}. Formally, there is a detection of O VI gas via the broad O VI 1031 transition, yet the continuum varies significantly near 1450Å in the STIS spectrum and the measured value is inconsistent with the upper limit implied by the O VI 1037 transition. In the following, we adopt the upper limit from the O VI 1037 transition.

TABLE 16
IONIC COLUMN DENSITIES FOR THE ABSORBER AT z=0.40570

Ion	λ (Å)	EW (mÅ)	AODM	N_{adopt}
HI				14.85 ± 0.05
CII	903.9616	< 13	< 12.92	< 12.92
CII	1036.3367	< 13	< 13.23	
CIII	977.0200	< 14	< 12.53	< 12.53
NII	1083.9900	< 16	< 13.32	< 13.32
NIII	989.7990	< 16	< 13.42	< 13.42
OII	834.4655	< 14	< 13.37	< 13.37
OIII	832.9270	< 15	< 13.50	< 13.50
OIV	787.7110	< 12	< 13.43	< 13.43
OVI	1031.9261	< 14	< 13.63	< 13.63
OVI	1037.6167	< 19	< 13.67	
SiIII	1206.5000	< 32	< 12.34	< 12.34

Assuming an equilibrium photoionization model with EUVB model Q, the upper limits to the observed ions constrain the metallicity of the gas as a function of the ionization parameter. In Figure 19, we plot the upper limit to the gas metallicity [M/H] for a range of U parameters. The plot symbols indicate the ion which places the most sensitive limit to [M/H]. For $\log U \approx -3$, the gas must have [M/H] < -1, but this would imply $n_H \approx 10^{-3}\,\mathrm{cm}^{-3}$ (for $J_{912} = 2 \times 10^{-23}$) which is considerably higher than expected for such a low N(HI) absorber. A more realistic value is $\log U \gtrsim -2$ for $N(\mathrm{HI}) = 10^{14.8}\,\mathrm{cm}^{-2}$ (§ 6.3) which implies [M/H] < -2 dex. The results indicate that this absorber has 5 to 100 times lower metal enrichment than the otherwise similar absorption system at $z = 0.36080$. Unless this absorber is a special example, systems with $N(\mathrm{HI}) \approx 10^{15}\,\mathrm{cm}^{-2}$ have large metallicity dispersion at these redshifts. We also note that a CIE model would imply even lower metallicities then the results shown in Figure 19.

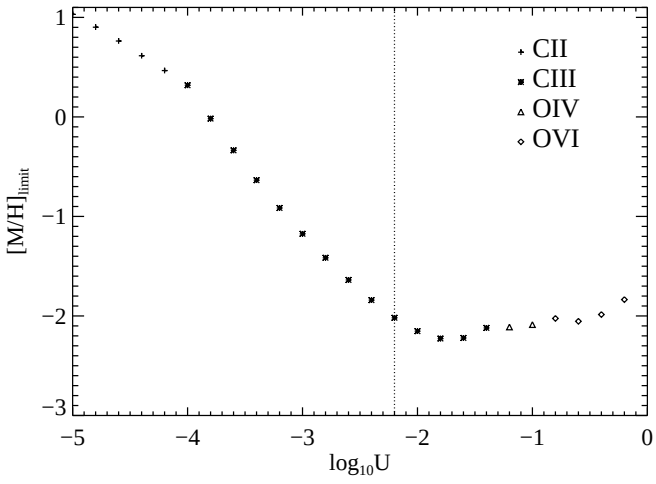

FIG. 19.— Upper limit to the metallicity of the absorber at $z = 0.40570$ as a function of ionization parameter. At each U value, the point style indicates the ion with the tightest constraint on the metallicity. For most of the parameter space, C III places the lowest limit to [M/H]. The dashed line indicates the likely ionization parameter for an absorber with $N(\mathrm{HI}) = 10^{14.8}\,\mathrm{cm}^{-2}$ (§ 6.3).

As an aside, we stress that C III places the tightest limit on the metal abundance for the largest range of parameter space. This ion and its corresponding C III 977 transition deserve greater attention in discussions of the Lyα forest. At higher redshift, the transition is frequently blended within the forest, yet we emphasize that it is a very powerful diagnostic of metal enrichment and ionization conditions within absorbers like the one at $z = 0.40570$ (c.f. Schaye et al. 2003).

In addition to the absorber at $z = 0.4057$, there are several absorbers with no unambiguous, statistically significant metal-line transitions. These are: $z = 0.030, N(\mathrm{HI}) = 10^{14.2}\,\mathrm{cm}^{-2}$; $z = 0.351, N(\mathrm{HI}) = 10^{14.2}\,\mathrm{cm}^{-2}$; $z = 0.409, N(\mathrm{HI}) = 10^{14.4}\,\mathrm{cm}^{-2}$; $z = 0.538, N(\mathrm{HI}) = 10^{14.2}\,\mathrm{cm}^{-2}$. In several cases, there are suggestions of metal-line absorption but line blending or poor S/N prevents a definitive measurement. In all cases, one can estimate an upper limit to their metal enrichment with an analysis similar to the one we performed for the $z = 0.40570$ system. Under the assumption of photoionization and assuming $\log U > -2$, we find [M/H] < -1.5 based on the non-detection of C III 977 and/or O VI and adopt this upper limit in the following discussion.

6. DISCUSSION

Section 4 presented a detailed analysis of the metal-line systems observed along the sightline to PKS0405–123. With the combined FUSE+STIS datasets, we have obtained constraints on the ionization mechanism, temperature, metallicity, and elemental abundance ratios of the gas. We summarize these properties in Table 17 which lists the redshift, N(HI) value, N(O VI) value, the ionization parameter, metallicity $[\mathrm{M/H}]_{phot}$, the total H column density N(H) assuming photoionization, the mean volume density n_H, and an estimate of the length scale ℓ assuming photoionization and $J_{912} = 2 \times 10^{-23}$ cgs. The table also lists the temperature and metallicity $[\mathrm{M/H}]_{coll}$ for collisionally ionized gas, and an estimate of N/α, the abundance of nitrogen relative to an α-element (e.g. Si, O). The following sub-sections consider various implications of our analysis on the nature of metal-line systems in the low redshift universe.

6.1. *Tracing the WHIM with O VI Absorbers*

As noted in the introduction, current theoretical expectation is that a significant fraction of baryons at $z < 1$ are in a warm-hot intergalactic medium (WHIM). One of the few means of detecting this gas is through O VI absorption. To this end, Tripp and collaborators have recently surveyed O VI gas along a number of quasar and AGN sightlines (Tripp et al. 2000; Savage et al. 2002). Their latest results indicate an incidence $dN_{\mathrm{O\,VI}}/dz = 14^{+9}_{-6}$ for an W$_\lambda$ limit of 50mÅ. This implies a baryonic mass density $\Omega_{\mathrm{O\,VI}} > 0.002 h_{75}^{-1}$ assuming the average metallicity

TABLE 17
SUMMARY TABLE

z	N(HI) (cm^{-2})	b_{HI}	N(OVI) (cm^{-2})	Ion[a]	$\log U$	$[\mathrm{M/H}]_{phot}$	$\log N(\mathrm{H})$ (cm^{-2})	n_H^c (10^{-5})	ℓ^c (kpc)	T_{coll} (10^5 K)	$[\mathrm{M/H}]_{coll}$	$[\mathrm{N}/\alpha]$
0.09180	14.5	38	13.8	??	> -1.5	> -1.4	18.8	< 2	> 90	> 2.5	> -2.2	
0.09658	14.7	40	13.7	Photo	-1.2	-1.5	19.2	1.2	440	–		
0.16710	16.5	38	14.8	Multi	-2.9	-0.25	18.8	60	3	–		$\gtrsim 0.2$
0.18250	14.9	27	< 13.8	??	–	–	–	–	$\lesssim -1$			
0.18290	14.1	26[b]	14.0	Coll	> -1	> -1	> 18.4	3	≈ -1.5			
0.36080	15.1	27	< 13.3	Photo	-2.0	> -0.7	18.6	8	16	–		-0.3
0.36332	13.4	–	13.4	Photo	-1.4	0	17.4	2	1			
0.49510	14.4	60[b]	14.3	Photo	-1.3	> -0.3	18.5	1.7	60	2.6	> -1	< -0.5

[a]This column lists the dominant ionization mechanism for the gas as inferred from the metal-line ratios. In several cases, the situation is ambiguous or multiple processes are required.
[b]There is a $> 25\%$ uncertainty in this value.
[c]These values assume $J_{912} = 2 \times 10^{-23}$ cgs.

is 0.1 solar and a very conservative ionization correction ($N(\mathrm{O\,VI})/N(\mathrm{O}) < 0.2$).

With the large redshift of PKS0405–123 and its extensive UV spectroscopy, we can derive O VI statistics for this sightline. We have detected six O VI systems to an W_λ limit of 30 mÅ over a non-contiguous redshift path of $\Delta z = 0.38$. This pathlength was determined by identifying all of the regions free of Galactic H_2 and other coincident transitions with sufficient S/N to identify and measure both members[11] of the O VI doublet to a 3σ W_λ threshold of 60 mÅ. We also searched for any O VI absorbers without corresponding Lyα absorption (to the same limit) and found no examples. Assuming Poisson statistics (e.g. Gehrels 1986), we find $dN_{\mathrm{O\,VI}}/dz = 16^{+9}_{-6}$ ($\pm 1\sigma$) which is consistent with Savage et al. (2002). If we combine our results with Savage et al. (2002) – ignoring the small difference in sensitivity – we find: $dN_{\mathrm{O\,VI}}/dz = 15^{+5}_{-4}$ ($\pm 1\sigma$).

An important aspect of the present work is that our observations place constraints on the ionization state and/or metallicity of several O VI absorbers. For the systems at $z = 0.09650, z = 0.36332$ and $z = 0.49510$, the detection of C III 977 precludes a single-phase CIE model and therefore suggests the gas is photoionized, in multiple ionization phases, or in a non-equilibrium state (see also Howk et al. 2004). If these absorbers have low temperature ($T < 10^5$ K), they are unlikely to contribute to the WHIM or present a significant reservoir of baryons. Future observations of the C IV profiles of these absorbers would be particularly valuable to address this issue. In contrast, the O VI gas in the absorbers at $z = 0.16710$ and $z = 0.18290$ are well modeled by a single-phase CIE model and we believe this gas is collisionally ionized. Finally, the absorber at $z = 0.09180$ is well modeled by both CIE and photoionization solutions. If the fraction of photoionized O VI absorbers is roughly half, then $\Omega_{\mathrm{O\,VI}}$ in the WHIM is roughly 50% the value that one would infer assuming all of the O VI gas is collisionally ionized. It will be important to examine the environment of the absorbers as a function of ionization state, e.g. to determine if the collisionally ionized gas arises preferentially in galactic halos (Sembach et al. 2003) or large-scale structures.

[11]Note that these selection criteria exclude the likely O VI system at $z = 0.08$ because the O VI 1037 transition is blended with a coincident transition.

Our analysis also constrains the metallicity of the gas giving rise to O VI absorption. For the absorbers presumed to be photoionized, the gas metallicity ranges from $[\mathrm{M/H}] \approx -1.5$ to 0 dex. The collisionally ionized gas shows systematically lower metallicity ($[\mathrm{O/H}] \approx -2$ to -1 dex) because this gas has much larger hydrogen ionization fraction. Altogether, these measurements are consistent with the values assumed and expected for O VI systems if the gas is related to the WHIM (e.g. Savage et al. 2002; Davé et al. 2001). It is worth noting, however, that several of the O VI lines are at the detection limit of this dataset and, therefore, absorbers with significantly lower metallicity would not have been detected. Unfortunately, it may not be possible with FUSE or HST/STIS to probe metallicities below $[\mathrm{O/H}] \approx -2$.

6.2. *Tracing the WHIM with Ne VIII Absorbers*

At temperatures $T > 5 \times 10^5$ K, O VI is no longer the dominant ion of oxygen. This is unfortunate because current simulations of the WHIM predict the bulk of the gas is at temperatures $T > 10^6$ K. For these reasons, X-ray spectroscopy of O VII and O VIII transitions offer a more direct probe of the WHIM (e.g. Fang et al. 2002) yet current technology allows a search for O VII and O VIII in only the brightest few X-ray sources. Even with the next generation of X-ray telescopes, surveys for O VII and O VIII will have limited impact. An alternative means of probing collisionally ionized gas with $T \gtrsim 10^6$ K is through the Ne VIII $\lambda\lambda 770, 780$ doublet. At these temperatures, Ne VIII is the dominant Ne ion and this relatively strong pair of transitions can be observed with FUSE and HST/STIS spectroscopy at $z > 0.2$. Specifically, FUSE spectroscopy with comparable spectral quality to the observations presented here will be sensitive to Ne VIII gas in absorbers with $\log N(\mathrm{HI}) + [\mathrm{M/H}] > 13$ for $10^{5.5}\,\mathrm{K} \lesssim T \lesssim 10^7\,\mathrm{K}$.

For sightlines with significant Galactic H_2 absorption (PKS0405–123 is a moderate example), a survey for Ne VIII is difficult for $\lambda < 1000$Å or $z < 0.3$. Nevertheless, we have conducted a search for Ne VIII absorption by examining the Ne VIII regions for all Lyα absorbers detected along the PKS0405–123 sightline. We found no significant detections. Furthermore, for $\lambda > 1000$Å we have found no pairs of absorption features with the appropriate separation of the Ne VIII doublet, independent of the presence of a corresponding Lyα feature. Altogether, we estimate the non-contiguous pathlength searched to be $\Delta z_{\rm Ne\,VIII} = 0.11$. Assuming Poisson statistics, we set a conservative 95% upper limit to the incidence of Ne VIII absorption: $dN_{\rm Ne\,VIII}/dz < 40$ for a 3σ rest-EW limit of ≈ 40mÅ. This result will be extended to lower W_λ limits and pursued along additional sightlines with forthcoming, approved FUSE programs (PI: Howk). We will also extend the analysis to include a search for Mg X absorption for systems with $z > 0.5$.

6.3. *Ionization of the IGM: A Possible N(H) Conspiracy*

The analysis described in § 4 allows us to investigate global trends in the ionization state of low z metal-line systems. One key result is that a significant fraction of the systems are predominantly photoionized. This is not a surprising result; current expectation is that the majority of the low z Lyα forest is photoionized gas (e.g. Davé & Tripp 2001). Unlike studies of the majority of Lyα 'clouds', however, an analysis of the metal-line systems provides an assessment of the ionization fraction and metallicity of this gas.

Focusing on the subset of systems where observations constrain the ionization state, we can examine trends between U and N(HI). Figure 20 presents a plot of $\log U$ vs $\log N$(HI) for all of the systems where we believe photoionization is the dominant mechanism. We caution, again, that in several cases the presumption of photoionization is not secure. In particular, the gas in the absorbers toward $z = 0.36332$ and $z = 0.49510$ may be in multiple ionization phases. In one case, we have only placed a lower limit to the U value; this is designated by the up arrow. Examining the figure, one notes a general decline in U with increasing N(HI). Performing the conservative generalized Spearman test, we calculate the significance to be 85%. Similarly, a Pearson test adopting the lower limit as a value rules out the null hypothesis at 97% c.l. and the results are more significant if we exclude the 'anomalous' absorber at $z = 0.36332$.

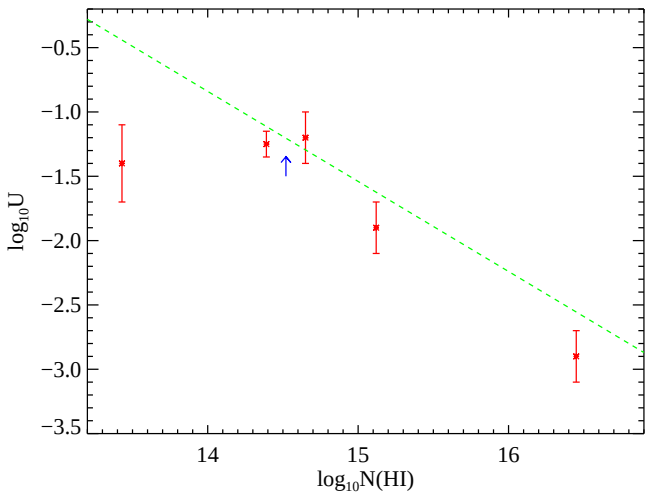

FIG. 20.— $\log U$ vs. $\log N$(HI) for the systems expected to be predominantly photoionized. The dashed line indicates a theoretical prediction based on comparisons between CDM numerical simulations and the low redshift Lyα forest (Davé & Tripp 2001).

Overplotted in the figure (dashed-line) is a prediction for the correlation between U and N(HI) at $z = 0.2$ derived in the following way. First, we adopt the Davé et al. (1999) relation between volume density n_H and N(HI) for low z Lyα absorbers:

$$1 + \delta \equiv \frac{\rho}{\bar{\rho}} = \frac{n_H}{\bar{n}_H} \propto N(\mathrm{HI})^{0.7} 10^{-0.4z} \qquad (2)$$

where

$$\bar{n}_H \equiv \mu \Omega_b \rho_c (1+z)^3 \qquad (3)$$

is the mean hydrogen density of the universe. Second, we assume a constant H I ionizing flux. This gives $U \propto N(\mathrm{HI})^{-0.7}$ and sets the slope of the dashed line in Figure 20. Finally, the normalization of the line is determined by assuming a value for the H I photoionization rate; the central value reported by Davé & Tripp (2001) from their analysis of the statistical properties of the $z < 1$ Lyα forest ($\Gamma_{HI} = 10^{-13.3}$ photons s^{-1} for $\bar{z} = 0.17$) gives the result shown here.

The correspondence between observation and theory is impressive. The curve is not a fit to the observations, it is a a comparison of prediction from numerical simulations with observed properties of the low z Lyα forest. It is especially noteworthy that the curve results from an analysis of the low z Lyα forest while our results are derived from the metal-line systems presented in this paper. Of course, the metal-line systems are simply a subset of the Lyα forest although the metal-line sample exhibits N(HI) values which exceed the principal range of the Davé et al. (1999) analysis. Furthermore, we caution that the majority of metal-line systems have $N(\mathrm{HI}) \approx 10^{14.5}$, i.e. the extremes of the parameter space described by Figure 20 are sparsely sampled. Nevertheless, the results presented in Figure 20 support the model of the IGM inferred from cosmological simulations.

Pushing the analysis one step further, we find a startling result regarding the total hydrogen column density N(H) of the low z Lyα forest. Examining Figure 21 and column 6 of Table 17, one notes that the predicted N(H) values for the metal-line systems based on photoionization modeling are nearly independent of N(HI). For all but one of the absorbers[12], $\log N(\mathrm{H}) = 18.75 \pm 0.3$ dex. While this result could be biased by our reliance on metal-line systems (e.g. lower N(H) systems may not be detected unless the gas had a very low ionization fraction), the roughly constant N(H) value is a natural consequence of the correlation between n_H and N(HI). Higher N(HI) implies higher n_H

[12]The one exception is the unusual O VI absorber at $z = 0.3633$ which shows a very weak Lyα profile apparently offset from the metal-line transitions. We include it here, but note its peculiar nature.

which implies lower U which implies a lower ionization fraction and, finally, a lower $N(\mathrm{H})/N(\mathrm{HI})$ ratio. In this manner, the correlation between n_H and $N(\mathrm{HI})$ can lead to a roughly constant $N(\mathrm{H})$ value.

The dashed line in Figure 21 presents the predicted $N(\mathrm{H})$ values as a function of $N(\mathrm{HI})$ assuming (1) the EUVB model Q at $z = 0.3$ and (2) $\log U = -3 - [N(\mathrm{HI})/10^{16.5}]^{\beta}$ with $\beta = 0.7$. The latter is equivalent to assuming a constant intensity for the EUVB radiation field and adopting the $n_H \propto N(\mathrm{HI})^{0.7}$ relation from Davé et al. (1999). We reach the unsettling conclusion that *all Lyα 'clouds' have roughly the same $N(\mathrm{H})$ value.* We stress that this result is sensitive to the value of β; larger ($\beta > 1$) or smaller ($\beta < 0.5$) values imply steeper relations between $N(\mathrm{H})$ and $N(\mathrm{HI})$. One seeks a physical interpretation – if it exists – for identifying $N(\mathrm{H}) \approx 10^{18.5-19}\,\mathrm{cm}^{-2}$ as a fundamental scale for the low redshift Lyα forest. This $N(\mathrm{H})$ value can be identified with a comoving length scale by adopting the mean hydrogen density of the universe at $z = 0$. Taking $\Omega_b = 0.04 h_{70}^{-2}$ (O'Meara et al. 2001), $N(\mathrm{H}) = 10^{19}\,\mathrm{cm}^{-2}$ corresponds to $\ell_{\mathrm{Ly}\alpha} \approx 17$ Mpc at $z = 0$. The observed variations in $N(\mathrm{HI})$, therefore, result from the compression of gas along this pathlength in overdense regions.

It is worth noting that the description of the IGM developed by Schaye (2001) based on Jeans length arguments also predicts a shallow dependence of $N(\mathrm{H})$ with n_H and $N(\mathrm{HI})$. In a future paper, we will investigate this $N(\mathrm{H})$ conspiracy through an analysis of numerical simulations and analytic arguments. If the near constancy of $N(\mathrm{H})$ is confirmed observationally, it could challenge models of the Lyα forest at $N(\mathrm{HI}) < 10^{16}\,\mathrm{cm}^{-2}$ which associate the 'clouds' with individual galaxies (e.g. galactic halos; Lanzetta et al. 1995; Chen et al. 1998; Chen, Lanzetta, & Webb 2001; Manning 2003).

In passing, we also note that because Davé et al. (1999) find $n_H \propto N(\mathrm{HI})^{0.7}$ to at least $z = 3$, one predicts the individual Lyα forest 'clouds' have a characteristic $N(\mathrm{H})$ at any given redshift from $z = 0-3$! The characteristic value of $N(\mathrm{H})$ does vary with redshift owing to evolution in the EUVB intensity, the redshift dependence of Equation 2, and the increasing density of the universe (Equation 3). In general, $N(\mathrm{H})$ is predicted to increase from $z = 0$ to $z = 3$.

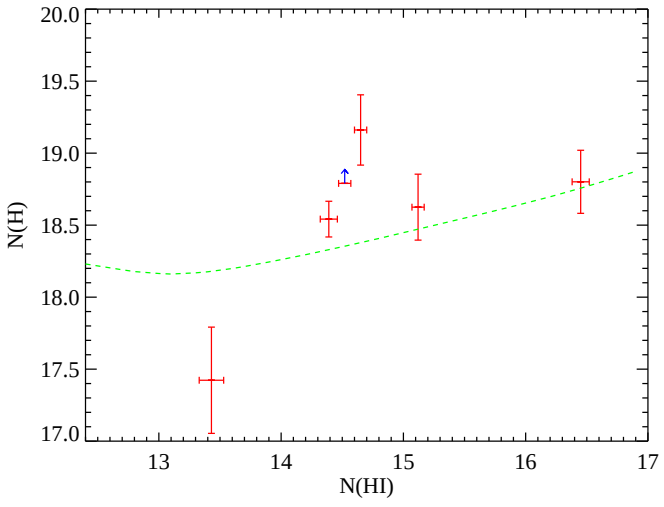

FIG. 21.— Inferred total hydrogen column densities $N(\mathrm{H})$ as a function of $N(\mathrm{HI})$ value for the metal-line systems toward PKS0405–123 which we believe are predominantly photoionized. The dashed line in Figure 20 maps to the dashed line shown here. Remarkably, both observation and theory suggest the Lyα forest clouds have roughly uniform $N(\mathrm{H})$ value for $N(\mathrm{HI}) = 10^{12-16}\,\mathrm{cm}^{-2}$.

Before concluding this sub-section, we note that we searched the literature for additional photoionized, metal-line systems to test the above conclusions. Unfortunately, this resulted in only two cases. One of these – the absorber at $z = 0.068$ toward PG0953+415 (Savage et al. 2002, ; $N(\mathrm{HI}) = 10^{14.35}\,\mathrm{cm}^{-2}$, $U = -1.35$) – has $N(\mathrm{HI})$ and U values which place it along the correlation expressed by the metal-line systems toward PKS0405–123 (Figure 20). Although the authors did not report an $N(\mathrm{H})$ value, adopting their ionization parameter we estimate $N(\mathrm{H}) = 10^{18.5}\,\mathrm{cm}^{-2}$. near $10^{18.5}\,\mathrm{cm}^{-2}$. The only other example is the absorber at $z = 0.0053$ toward 3C 273 which lies within the Virgo supercluster (Tripp et al. 2002). Taking their single-phase solution, this absorber falls below the relation in Figure 20, although its unique surroundings may imply an unusual physical environment (Stocke et al. 2004). It may also be noteworthy that the two outliers from the U, $N(\mathrm{HI})$ relation fall beneath the curve. This is consistent with the results of Davé et al. (1999) who emphasized the simulations show a significant scatter in the $1 + \delta \propto N(\mathrm{HI})^{0.7}$ correlation at low z with the majority of 'outliers' identified above the relation (i.e. lower U).

6.4. *Chemical Enrichment of the Low z IGM*

An active area of current research is the study of the chemical enrichment of the IGM (e.g. Songaila 2001; Pettini et al. 2003; Schaye et al. 2003). These studies test scenarios of Population III star formation (e.g. Gnedin & Ostriker 1997; Wasserburg & Qian 2000) as well as feedback processes in early galaxy formation (Aguirre et al. 2001). Preliminary studies with 10m-class telescopes argued for significant enrichment in Lyα 'clouds' with $N(\mathrm{HI}) > 10^{14}\,\mathrm{cm}^{-2}$ (Tytler et al. 1995) but a stacked spectrum of lower H I systems showed no corresponding C IV absorption (Lu et al. 1998). Recently, analyses of the 'pixel technique' have argued for metal enrichment to very low overdensity (e.g. Ellison et al. 2000). Recently, Schaye et al. (2003) have argued that the Lyα forest has a median carbon metallicity $[\mathrm{C/H}] = -3.47^{+0.07}_{-0.06} + 0.08^{+0.09}_{-0.10}(z-3) + 0.65^{+0.10}_{-0.14}(\log\delta - 0.5)$ where δ is the overdensity of the gas and is related to $N(\mathrm{HI})$ as described in Equations 2,3. Simcoe, Sargent, & Rauch (2004) have reached similar conclusions, although with ≈ 0.3 dex higher values for [O/H] and a less dramatic dependence on overdensity[13]. Very little research, in comparison, has been pursued at low redshift. Burles & Tytler (1996) surveyed O VI absorbers at $z \sim 1$ and argue that the metallicity in these systems is $[\mathrm{O/H}] \geq -2.4$ dex. Similarly, Barlow & Tytler (1998) examined a large sample of C IV absorbers and found a mean metallicity $[\mathrm{C/H}] \approx -1.5$ dex. These results, imply higher enrichment levels within the Lyα forest at low z and therefore a significant evolution in the chemical enrichment of the IGM.

[13]These differences are primarily due to the fact that the authors' fiducial models assumed EUVB radiation fields with differing spectral shapes.

The analysis presented in this paper (summarized in Table 17) can be used to evaluate the chemical abundances of the low z Lyα forest for comparison with high z. We will focus here on absorbers with $\log N(\mathrm{HI}) > 14$ which includes the absorbers without significant metal-line transitions (§ 5). For the systems with detectable metal-line absorption, the median metallicity lies at $\approx 1/10$ solar enrichment if the absorbers are predominantly photoionized. A significant fraction of these absorbers exhibit chemical enrichment comparable to the Milky Way and its Magellanic Clouds. Another significant result is the large scatter in chemical enrichment among the absorbers. The systems span at least two decades in metallicity ranging from approximately solar metallicity to $< 1/100$ solar. Although UV spectroscopy has poorer resolution and S/N than optical spectra, we emphasize that the relatively high metallicities derived here are not the result of observational bias. For most of the systems, these transitions are saturated or detected well above threshold. If this gas had $10\times$ lower metallicity, several transitions would still be detectable, although constraints on the ionization state would be weaker. If we include the ≈ 5 absorbers without significant metal-line absorption and assume their enrichment is below -1.5 dex, then the median metallicity lies closer to 1/30 solar. In either case, the median metallicity is consistent with the results presented by Barlow & Tytler (1998) based on their analysis of C IV absorption in the $z \sim 0.5$ Lyα forest.

Altogether, the results from the PKS0405–123 sightline indicate that Lyα clouds with $N(\mathrm{HI}) > 10^{14}\,\mathrm{cm}^{-2}$ show a median value of $1/30 - 1/10$ solar and a log normal dispersion of ≈ 1 dex. This median metallicity is significantly higher than the value ascribed to Lyα 'clouds' with comparable $N(\mathrm{HI})$ values at high z (e.g Songaila 2001; Schaye et al. 2003). In fact, the value and scatter are remarkably similar to values derived for $z \approx 2$ damped Lyα systems (e.g. Prochaska et al. 2003). Within the CDM paradigm, however, the 'clouds' in the low redshift Lyα forest have much higher overdensity δ compared to high z Lyα clouds. If a correlation between metallicity and overdensity exists, we must be careful to compare metallicities at the same overdensity. We can derive the metallicity of absorbers with comparable overdensity in the $z \sim 3$ universe by (i) calculating $1+\delta$ for an absorber with $N(\mathrm{HI}) = 10^{14.5}\,\mathrm{cm}^{-2}$ using Equation 2 and (ii) evaluating the metallicity [C/H] at this overdensity using the results presented by Schaye et al. (2003). We find [C/H] $= -2.9$ at $z = 3$ with a log normal scatter of 0.55 dex. This metallicity and scatter are lower than the sample of absorbers analyzed in this paper. Even if we adopt non-solar relative abundances (e.g. [Si/C] $= +0.7$; Aguirre et al. 2004), the metallicity of these low z Lyα absorbers greatly exceeds absorbers with comparable overdensity at high redshift.

In short, our observations suggest a significant enrichment of the $\delta \approx 20$ IGM between $z = 3$ and the present universe. This is in stark contrast to current claims that the IGM has at most a moderate metal enrichment from $z = 2$ to 5 (Songaila 2001; Pettini et al. 2003; Schaye et al. 2003). Of course, our range of redshifts corresponds to ≈ 10 Gyr wherein significant galactic enrichment has occurred. It apparently requires that the overdense IGM is polluted by processes related to galaxy formation, e.g., winds driven by supernovae and/or mergers (e.g. Cox et al. 2004). By inference, this weakens arguments that the IGM has been enriched primarily by an initial generation of Population III stars (e.g. Gnedin & Ostriker 1997; Wasserburg & Qian 2000), although it does not preclude the occurrence of both early and ongoing enrichment.

Given a correlation exists between $N(\mathrm{HI})$ and n_H, one might expect correlations between $N(\mathrm{HI})$ and metallicity. For example, regions of higher overdensity will on average be closer to galaxies and therefore may be at higher metallicity than less dense gas. As noted above, Schaye et al. (2003) report a correlation between metallicity and overdensity when matching their simulations against C IV absorption in the high z Lyα forest. In the sample of $z < 0.5$ metal-line systems toward PKS0405–123, however, there is no obvious correlation between $N(\mathrm{HI})$ and metallicity. While the partial LLS at $z = 0.16710$ does show near solar abundance, the lower $N(\mathrm{HI})$ absorbers at $z = 0.49510$ and 0.36080 have comparable metallicity. Furthermore, there is no apparent correlation of metallicity with ionization parameter or redshift. Because these conclusions are based on a small sample, an underlying trend may be masked by only a few outliers or systematic effects. A goal of future studies will be to obtain complete observations for a sample of $N > 20$ absorbers with a wide range of $N(\mathrm{HI})$ values.

In a smaller sample of the PKS0405–123 metal systems, we were able to constrain the N/O or N/Si relative abundance. Table 17 summarizes these results. The majority of absorbers are consistent with the general pattern of N/O values expressed by local measurements of H II regions and stars (Henry, Edmunds, & Köppen 2000). The obvious exception is the absorber at $z = 0.49510$ which shows a super-solar metallicity and an upper limit to N/O of -0.6 dex under the assumption of photoionization. The low N/O value is characteristic of the values measured in starbursting galaxies (e.g. Contini et al. 2002) and suggests this gas was enriched by an outflow from such a system. Future observations of N V and a deeper search for galaxies at $z = 0.495$ will help clarify this picture.

7. SUMMARY

We have presented an analysis of nine metal-line absorption systems toward PKS0405–123 using the combination of *FUSE* and HST/STIS ultraviolet spectroscopy. We derive H I column densities $N(\mathrm{HI})$ from curve-of-growth analyses and examine ionic ratios to constrain the ionization mechanism of the gas. These ratios are compared against single-phase model predictions for collisional ionization and photoionization to constrain the temperature and/or ionization parameter U and thereby infer physical conditions of the absorber (density, metallicity, ionization fraction).

We identify six O VI absorbers to a 3σ equivalent width limit of 30mÅ along a non-contiguous redshift path $\Delta z_{\mathrm{O\,VI}} = 0.38$. This gives $dN/dz|_{\mathrm{O\,VI}} = 16 \pm 6$, consistent with other low z sightlines. These systems exhibit metallicities [O/H] from -1.5 to 0 dex which roughly matches prediction for the warm-hot intergalactic medium (WHIM). Half of the O VI absorbers, however, show transitions which suggest the gas is photoionized or has multiple ionization phases. This may argue against their membership in the WHIM, although a quantitative assessment awaits a careful as-

sessment of the ionization state of the gas in the numerical simulations. We also survey the WHIM through a search for Ne VIII absorbers which should probe gas at temperatures $T \approx 10^6$ K. Over a non-contiguous pathlength $\Delta z_{\rm Ne\,VIII} = 0.11$ we find no such systems and estimate $dN/dz|_{\rm Ne\,VIII} < 40$ to an 3σ equivalent width limit of ≈ 40mÅ.

The photoionized metal-line systems show decreasing ionization parameter with increasing N(HI) value. Both the slope and normalization of this correlation match a prediction derived from previous analysis of the Lyα forest with cosmological simulations (Davé & Tripp 2001). This correspondence lends support to paradigm of the IGM described by numerical simulations. Furthermore, the observed and predicted U vs. N(HI) correlation imply a startling 'N(H) conspiracy': the entire population of Lyα clouds have roughly identical total hydrogen column density, i.e. independent of N(HI). We argue this conspiracy holds at all redshifts although with the characteristic N(H) value increasing with redshift.

The median metallicity of absorbers with $N({\rm HI}) > 10^{14}\,{\rm cm}^{-2}$ is $\approx 1/30 - 1/10$ solar metallicity with a large (≈ 1 dex) dispersion. This metallicity is consistent with a previous analysis of the low z Lyα forest and indicates a significant enrichment of the IGM since $z \sim 2$. There is no obvious correlation between metallicity and any other physical property of the gas. Finally, we present a small sample of N/O measurements which are generally consistent with H II regions and stars of comparable metallicity.

This work is based on observations obtained by the NASA-CNES-ESA *FUSE* mission, operated by Johns Hopkins University. It is also based on observations with the NASA/ESA *Hubble Space Telescope* obtained at the Space Telescope Science Institute, which is operated by the Association of Universities for Research in Astronomy, Inc., under NASA contract NAS5-26555. The authors wish to thank P. Madau, A. Aguirre, and R. Davé for helpful discussions. This work was supported by a FUSE GI grant to JXP, HWC, and BJW under NASA contract NAG5-12743. HWC also acknowledges support by NASA through a Hubble Fellowship grant HF-01147.01A from the Space Telescope Science Institute, which is operated by the Association of Universities for Research in Astronomy, Incorporated, under NASA contract NAS5-26555. Finally, JCH acknowledges support to NASA contract NAG5-12345.

REFERENCES

Adelberger, K.L., Steidel, C.C., Shapley, A.E., & Pettini, M. 2003, ApJ, 584, 45
Aguirre, A., Hernquist, L., Schaye, J., Katz, N., Weinberg, D.H., & Gardner, J. 2001, ApJ, 561, 521
Aguirre, A., Schaye, J., Kim, T.-S., Theuns, T., Rauch, M., & Sargent, W.L.W. 2004, ApJ, 602, 38
Barlow, T. & Tytler, D. 1998, AJ, 115, 1725
Bentz, M.C., Hall, P.B., & Osmer, P.S. 2004, AJ, submitted (astro-ph/0402205)
Bergeson, S.D. & Lawler, J.E. 1993, ApJ, 408, 382
Bergeson, S.D. & Lawler, J.E. 1993b, ApJ, 414, L137
Bergeson, S.D., Mullman, K.L., & Lawler, J.E. 1993, ApJ, 435, L157
Bergeson, S.D., Mullman, K.L., & Lawler, J.E., 1996, ApJ464, 1050
Burles, S. & Tytler, D. 1996, ApJ, 460, 584
Cen, R. & Ostriker, J.P. 1999, ApJ, 514, 1
Chen, H.-W., Lanzetta, K. M., Webb, J. K., & Barcons, X. 1998, ApJ, 498, 77
Chen, H.-W., Lanzetta, K. M., & Webb, J. K. 2001,ApJ, 556, 158
Chen, H.-W. & Prochaska, J.X. 2000, ApJ, 543, L9
Chen, H.-W., et al. 2004, in preparation
Contini, T., Treyer, M.A., Sullivan, M., & Ellis, R.S. 2002, MNRAS, 330, 75
Cox, T.J., Primack, J., Johnsson, P., & Somerville, R. 2004, ApJ, submitted (astro-ph/0402675)
Davé, R., Hernquist, L., Katz, N., & Weinberg, D.H., 1999, ApJ, 511, 521
Davé, R. & Tripp, T.M. 2001, ApJ, 553, 528
Davé, R., Cen, R., Ostriker, J.P., Bryan, G.L., Hernquist, L., Katz, N., Weinberg, D.H., Norman, M., & O'Shea, B. 2001, ApJ, 552, 473
Ellison, S.L., Songaila, A., Schaye, J., & Pettini, M. 2000, AJ, 120, 1175
Fang, T. & Bryan, G.L. 2001, ApJ, 561, 31L
Fang, T., Marshall, H.L., Lee, J.C., Davis, D.S., & Canizares, C.R. 2002, ApJ, 572, L127
Fedchak, J. A. & Lawler, J. E. 1999, ApJ, 523, 734
Fedchak, J. A., Wiese, L. M., & Lawler, J. E. 2000, ApJ, 538, 773
Ferland, G. J. 2001, PASP, 113, 41
Gehrels, N. 1986, ApJ, 303, 336
Gnedin, N.Y. & Ostriker, J.P. 1997, ApJ, 486, 581
Gnedin, N. Y., & Hui, L. 1998, MNRAS, 296, 44
Grevesse, N. & Sauval, A.J. 1999, A&A, 347, 348
Haardt, F. & Madau, P. 1996, ApJ, 461, 20
Haardt, F. & Madau, P. 2004, in preparation
Henry, R.B.C., Edmunds, M.G., & Köppen, J. 2000, ApJ, 541, 660
Holweger, H. 2001, in Solar and Galactic Composition, ed. R.F. Wimmer-Schweingruber, (Berlin: Springer), 23
Howk, J.C., Sembach, K.R., Roth, K.C., & Kruk, J.W. 2000, ApJ, 544, 867
Howk, J.C., et al. 2004, in preparation
Jenkins, E. B. 1996, ApJ, 471, 292
Lanzetta, K.M., Bowen, D.V., Tytler, D., & Webb, J.K. 1995, ApJ, 442, 538
Linder, S. M. 2000, ApJ, 529, 644
Lu, L., Sargent, W.L.W., Barlow, T.A., Churchill, C.W., & Vogt, S. 1996, ApJS, 107, 475
Lu, L., Sargent, W.L.W., Barlow, T.A., & Rauch, M. 1998, astro-ph/9802189
Manning, C.V. 2003, ApJ, 595, 19
Miralda-Escudé, J., Cen, R., Ostriker, J.P., & Rauch, M. 1996, ApJ, 471, 582
Moos, H.W., et al. 2000, ApJ, 538, L1
Morton, D.C. 1991, ApJS, 77, 119
Morton, D.C. 2004, priv. comm.
O'Meara, J.M., Tytler, D., Kirkman, D., Nao, S., Prochaska, J.X., Lubin, D., & Wolfe, A.M. 2001, ApJ, 552, 718
Osmer, P.S. 1980, ApJ, 237, 666
Pettini, M., Smith, L.J., King, D.L., & Hunstead, R.W. 1997, ApJ, 486, 665
Pettini, M., Madau, P., Bolte, M., Prochaska, J.X., Ellison, S.L., & Fan, X. 2003, ApJ, 594, 695
Prochaska, J.X., Howk, J.C., & Wolfe, A.M. 2003, Nature, 423, 57
Prochaska, J.X., Gawiser, E., Wolfe, A.M., Castro, S., & Djorgovski, S.G. 2003, ApJ, 595, L9
Prochaska, J.X. et al. 2004, in preparation
Prochaska, J.X. & Davé, R. 2004, in preparation
Sahnow, D.J., et al. 2000, ApJ, 538, L7
Sargent, W.L.W., Steidel, C.C., & Boksenberg 1998, ApJS, 68, 539
Savage, B. D. and Sembach, K. R. 1991, ApJ, 379, 245
Savage, B.D., Sembach, K.R., Tripp, T., & Richter, P. 2002, ApJ, 564, 631
Schaye, J. 2001, ApJ, 559, 507
Schaye, J., Aguirre, A., Kim, T.-S., Theuns, T., Rauch, M., & Sargent, W.L.W. 2003, ApJ, 596, 768
Schectman, R.M., Povolny, H.S., & Curtis, L.J. 1998, ApJ, 504, 921
Sembach, K.R., Wakker, B.P., Savage, B.D., Richter, P., Meade, M., Shull, J.M., Jenkins, E.B., Sonneborn, G., & Moos, H.W. 2003, ApJS, 146, 165
Simcoe, R.A., Sargent, W.L.W., & Rauch, M. 2002, ApJ, 578, 737
Simcoe, R.A., Sargent, W.L.W., & Rauch, M. 2004, ApJ, in press (astro-ph/0312467)
Songaila, A. 2001, ApJ, 568, L139
Spitzer, L., Jr. 1996, ApJ, 458, L29
Stocke, J.T., Keeney, B.A., McLin, K.M., Rosenberg, J.L., Weymann, R.J., & Giroux, M.L. 2004, ApJ, in press (astro-ph/0403042)
Sutherland, R.S. & Dopita, M.A. 1993, ApJS, 88, 253
Tripp, T. M., Lu L., & Savage B.D. 1996, ApJS, 102, 239
Tripp, T. M., Savage B.D., Jenkins, E.B. 2000, ApJ, 534, L1
Tripp, T.M. et al. 2002, ApJ, 575, 697

Tytler, D. et al. 1995, in QSO Absorption Lines, ESO Astrophysics Symposia, ed. G. Meylan (Springer, Heidelberg), p. 289
Verner, D. A., Barthel, P. D., Tytler, D. 1994, A&AS, 108, 287
Vogel, S. & Reimers, D. 1995, A&A, 294, 377
Wasserburg, G.J. & Qian, Y.-Z. 2000, ApJ, 538, L99
Wiese, L.M., Fedchak, J. A., & Lawler, J. E. 2001, ApJ, 547, 1178
Williger, G. et al. 2004, in preparation
Woosley, S.E. & Weaver, T.A. 1995, ApJS, 101, 181
Zhang, Y., Anninos, P., Norman, M.L., & Meiksin A. 1997, ApJ, 485, 496